JEM Journal of Experimental Medicine

ARTICLE

EP3 enhances adhesion and cytotoxicity of NK cells toward hepatic stellate cells in a murine liver fibrosis model

Xixi Tao[1*], Rui Zhang[1*], Ronglu Du[1*], Tingting Yu[1*], Hui Yang[2], Jiwen Li[2], Yuhong Wang[1], Qian Liu[1], Shengkai Zuo[1], Xi Wang[3], Michael Lazarus[4], Lu Zhou[2], Bangmao Wang[2], Ying Yu[1], and Yujun Shen[1]

Natural killer (NK) cells exhibit antifibrotic properties in liver fibrosis (LF) by suppressing activated hepatic stellate cell (HSC) populations. Prostaglandin E_2 (PGE_2) plays a dual role in innate and adaptive immunity. Here, we found that E-prostanoid 3 receptor (EP3) was markedly downregulated in NK cells from liver fibrosis mice and patients with liver cirrhosis. NK cell–specific deletion of EP3 aggravated hepatic fibrogenesis in mouse models of LF. Loss of EP3 selectively reduced the cytotoxicity of the $CD27^+CD11b^+$ double positive (DP) NK subset against activated HSCs. Mechanistically, deletion of EP3 impaired the adhesion and cytotoxicity of DP NK cells toward HSCs through modulation of Itga4-VCAM1 binding. EP3 upregulated Itga4 expression in NK cells through promoting Spic nuclear translocation via PKC-mediated phosphorylation of Spic at T191. Activation of EP3 by sulprostone alleviated CCL4-induced liver fibrosis in mice. Thus, EP3 is required for adhesion and cytotoxicity of NK cells toward HSCs and may serve as a therapeutic target for the management of LF.

Introduction

Chronic liver injuries caused by hepatitis virus infection, alcoholic or nonalcoholic steatohepatitis, and biliary obstruction lead to pathologic fibrogenesis and further to liver fibrosis (LF), which eventually leads to cirrhosis and liver failure (Kisseleva and Brenner, 2021). Although the fibrotic condition is potentially reversible after removal of the etiological sources (Ellis and Mann, 2012), disease regression was not observed in a substantial percentage of patients with advanced cirrhosis (Marcellin et al., 2013). During LF progression, activated hepatic stellate cells (HSCs) play a pivotal role in fibrotic tissue deposition. HSCs are perisinusoidal-resident, vitamin A–storing cells that undergo phenotypic transformation into profibrogenic myofibroblasts (activated) upon stimulation by various inflammatory cytokines and mediators. Pharmacological and genetic inhibition of HSC transition and proliferation provide promising therapeutic strategies against hepatic fibrosis (Higashi et al., 2017).

Accumulated evidence has demonstrated that both innate and adaptive immune cells can interact with HSCs and trigger both pro- and antifibrotic responses to maintain liver homeostasis (Pellicoro et al., 2014). Generally, $CD8^+$ (Taylor et al., 2018) and B cells (Faggioli et al., 2018; Novobrantseva et al., 2005) exhibit profibrotic properties, while macrophages (Tacke and Zimmermann, 2014), natural killer (NK) T (Park et al., 2009; Wehr et al., 2013), $CD4^+$ (Glassner et al., 2013; Shen et al., 2017), and dendritic cells (DCs; Lukacs-Kornek and Schuppan, 2013) play dual roles in HSC activation and LF. In particular, NK cells display a distinctive antifibrotic capability by directly killing early activated or senescent HSCs (Krizhanovsky et al., 2008) or by induction of HSC apoptosis (Fasbender et al., 2016), which may have therapeutic potential in fibrotic diseases (Rurik et al., 2022). NK cell–mediated cytotoxicity is governed by a coordinated series of steps composed of recognition (contact and adhesion), effector degranulation and lysis, and termination (detachment; Mace et al., 2014). During the recognition process, tight adhesion to the target cells is indispensable for cytolysis by NK cells (Helander and Timonen, 1998). Some studies have shown that NK cells can interact with activated HSCs expressing

[1]Department of Pharmacology, Tianjin Key Laboratory of Inflammatory Biology, Center for Cardiovascular Diseases, Key Laboratory of Immune Microenvironment and Disease (Ministry of Education), The Province and Ministry Co-sponsored Collaborative Innovation Center for Medical Epigenetics, School of Basic Medical Sciences, Tianjin Medical University, Tianjin, China; [2]Department of Gastroenterology and Hepatology, Tianjin Medical University General Hospital, Tianjin Institute of Digestive Diseases, Tianjin Key Laboratory of Digestive Diseases, Tianjin, China; [3]Department of Immunology, School of Basic Medical Sciences, Capital Medical University, Beijing, China; [4]International Institute for Integrative Sleep Medicine, University of Tsukuba, Tsukuba City, Ibaraki, Japan.

*X. Tao, R. Zhang, R. Du, and T. Yu contributed equally to this paper. Correspondence to Yujun Shen: yujun_shen@tmu.edu.cn.

RAE-1 (Radaeva et al., 2007) and TRAIL (TNFα-related apoptosis inducing ligand; Glassner et al., 2012) by activating receptors, such as NKG2D (Radaeva et al., 2006) and NKp46 (Gur et al., 2012). Cell–cell adhesion is the key step in NK cell cytotoxicity against activated HSCs (Melhem et al., 2006; Muhanna et al., 2008). However, the mechanism underlying the adhesion between NK cells and HSCs is still not fully understood. In NK cells, multiple integrins (αLβ2, α4β1, etc.) mediate adhesive interactions with their cognate ligands such as ICAM (intercellular adhesion molecule) and VCAM1 on target cells (Shannon and Mace, 2021), but whether integrin-ligand binding mediates adhesion and cytolysis of HSCs by NK cells in LF remains unknown.

Prostaglandins (PGs) are potent bioactive lipids, derived from arachidonic acid through the sequential reaction of cyclooxygenases and PG synthases. PGs, including PGE_2, PGD_2, $PGF_{2\alpha}$, PGI_2, and thromboxane A_2, exert multiple biological actions by binding to their own G protein–coupled receptors: EP (EP1, EP2, EP3, EP4), DP (DP1, DP2), FP, IP, and TP (Harizi et al., 2008). Each of the receptors couples to unique complements of signaling cascades such as Ca^{2+} and cAMP signaling in a cell type–specific manner. PGE_2 plays a dual role in the modulation of innate and adaptive immunity (depending on the context) and target cells. For example, PGE_2/EP2 signaling suppresses macrophage maturation (Zaslona et al., 2012), while the PGE_2/EP3 axis promotes cardiac healing after myocardial infarction by activating reparative macrophages (Tang et al., 2017). PGE_2 is required for DC maturation with costimulatory molecules for T cell proliferation (Krause et al., 2009), whereas pharmacological blockade of PGE_2 biosynthesis enhances DC-dependent priming of T cell responses (Hayashi et al., 2020). Additionally, PGE_2 suppresses or enhances Th1 cell IFN-γ production depending on the mature status of the cell (Betz and Fox, 1991; Yao et al., 2009). NK cells express all PGE_2 receptors (EP1–4) (Holt et al., 2011; Holt et al., 2012; Martinet et al., 2010). PGE_2 receptors EP2 and EP4 suppress NK cell function in a variety of contexts (Bottcher et al., 2018; Galland et al., 2017). However, a recent study showed that PGE_2 dramatically enhances the tumor-infiltrating and killing capacity of a distinct subpopulation of $CD25^+CD54^+$ NK cells (Chen et al., 2021). Whether and how PGE_2 receptors regulate NK cell function in LF remains to be elucidated.

In this study, we found that EP3 expression was downregulated in blood NK cells from patients with liver cirrhosis and hepatic NK cells in mouse models of LF. NK cell–specific deletion of EP3 aggravated carbon tetrachloride (CCL4)– and bile duct ligation (BDL)–induced LF in mice, with decreased cytotoxicity in the $CD27^+CD11b^+$ double-positive (DP) NK subset toward activated HSCs. Adoptive transfer of DP NK cells attenuated CCL4-induced LF in EP3-deficient mice. Mechanically, EP3 activation enhanced adhesion and cytotoxicity of DP NK cells to HSCs through promoting Itga4 binding with VCAM1 on HSCs. EP3 transcriptionally upregulated Itga4 expression in NK cells through Ca^{2+}/protein kinase C (PKC)/Spic signaling. Treatment of EP3 agonist attenuated LF in mice. Collectively, our findings unveil a protective role of EP3 against LF through enhancing adhesion and cytotoxicity of DP NK cells toward HSCs.

Results

Inhibition of EP3 receptor suppresses cytotoxicity of mouse NK cells toward HSCs

Intrahepatic NK activity is significantly decreased in patients with advanced LF (Mele et al., 2021) and animal models of LF (Melhem et al., 2006). To explore the function of PG receptors in NK cells in LF, we first profiled the expression of PG receptors in hepatic NK cells derived from BDL and CCL4-treated mice and observed a consistent decrease in *EP3* and *EP4* expression in hepatic NK cells in both LF models (Fig. 1, A and B). After treatment with selective inhibitors of EP (SC-51322 for EP1; PF-04418948 for EP2; L-798,106 for EP3; and L161,982 for EP4), TP (SQ29548), and FP (AL8810), NK cells were subjected to activated HSCs. Notably, blockage of EP3 had the strongest inhibitory effect on the cytotoxic activity of NK cells against activated primary mouse HSCs (Fig. 1 C), and EP3 inhibitor also suppressed the cytotoxic capacity of primary splenic and hepatic NK cells in a dose-dependent manner (Fig. 1, D and E). Moreover, we also observed downregulated EP3 protein expression in hepatic NK cells form fibrotic livers of HA-tagged EP3 transgenic mice (Fig. 1, F and G). Finally, NK cells isolated from spleens and livers of EP3 global knockout ($EP3^{-/-}$) mice recaptured the impaired cytotoxicity of NK cells toward HSCs induced by EP3 inhibitor (Fig. 1, H and I). These results indicate that the loss of EP3 might compromise NK cell function in LF.

EP3 ablation in NK cells aggravates, while EP3 overexpression attenuates, CCL4-induced LF in mice

Based on the decreased NK cell activity in $EP3^{-/-}$ mice, we examined the role of EP3 in NK cells during LF. H&E staining, hydroxyproline assay, and Sirius red staining revealed that 4 wk of repeated exposure to CCL4 led to more severe liver injury and increased collagen deposition in $EP3^{-/-}$ mice compared with WT mice (Fig. S1, A–C), as detected by increased hepatic protein levels of fibrosis markers α-SMA and Col III, and HSC marker desmin (Fig. S1, D and E). Again, NK cell–specific deletion of EP3 ($EP3^{F/F}NKp46^{Cre}$; Fig. 2, A–E) aggravated hepatic fibrogenesis in mice in both CCL4-treated (Fig. 2, F–J) and BDL models (Fig. 2, K–O). In contrast, conditional overexpression of the major isoform EP3α (Fig. S1, F and G) in mouse NK cells (Fig. S1 H) significantly attenuated CCL4-induced LF in mice (Fig. S1, I–M). Thus, EP3 is essential for the antifibrotic activity of NK cells in LF.

EP3 deficiency aggravates CCL4-induced LF in mice through suppression of DP NK cell activity

NK cells are a heterogeneous population in terms of their surface marker profile, function, and anatomic distribution. In mice, maturation of NK cells is a four-stage developmental program: $CD27^-CD11b^-$ (double-negative [DN]) → $CD27^+CD11b^-$ (CD27 single positive [SP]) → $CD27^+CD11b^+$ (DP) → $CD27^-CD11b^+$ (CD11b SP). Loss of EP3 in NK cells had no overt influence on the total percentage and number of NK cells in the spleen (Fig. 3, A–C) and liver (Fig. 3, D–F). However, compared with $EP3^{F/F}$ mice, there was a significantly reduced ratio and number of DP NK subsets in spleen (Fig. 3, G–I) and liver (Fig. 3, J–L) in $EP3^{F/F}NKp46^{Cre}$ mice, whereas the DN NK cell ratio was

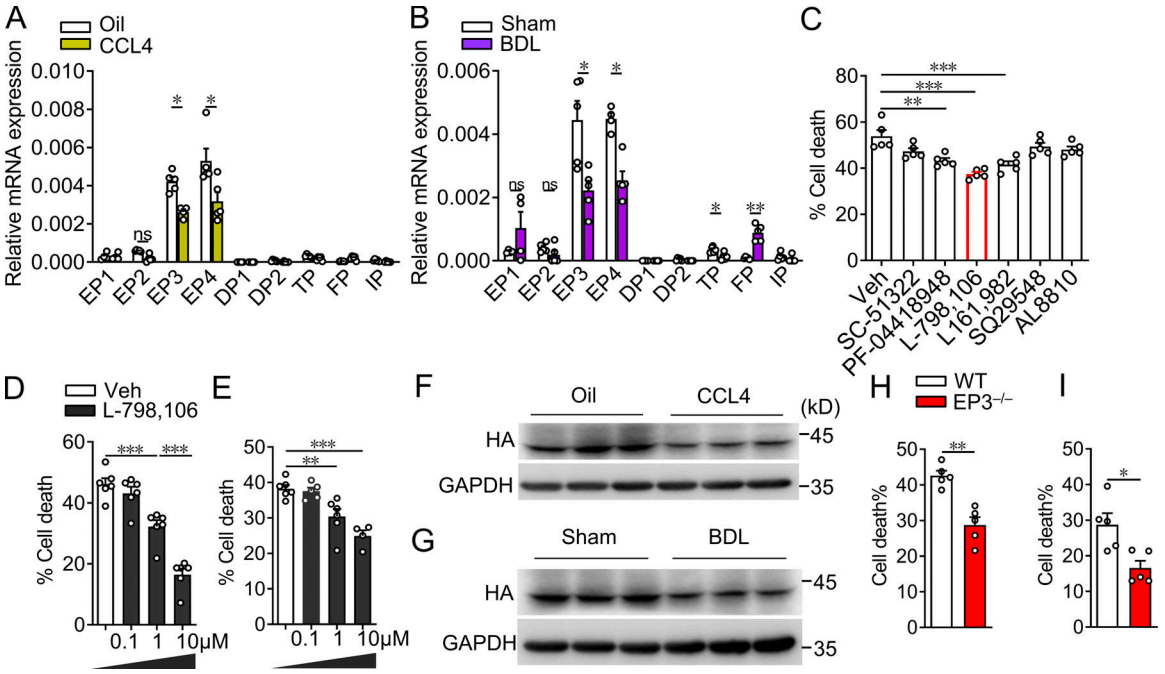

Figure 1. **Inhibition of EP3 decreases mouse NK cell cytotoxicity against activated HSCs. (A)** The expression profile of PG receptors in primary NK cells from livers of CCL4-treated mice (n = 4–5 per group). **(B)** The expression profile of PG receptors in primary NK cells from livers of BDL mice (n = 4–5 per group). **(C)** Primary NK cells from mouse spleen were tested for cytotoxicity against activated mouse HSCs (NK:HSC = 10:1) after treatment of inhibitors of PG receptors (SC-51322 for EP1; PF-04418948 for EP2; L-798,106 for EP3; L161,982 for EP4; SQ29548 for TP; and AL8810 for FP; n = 5 per group). **(D and E)** Dose-dependent effect of EP3 inhibitor L-798,106 on mouse splenic (D) and hepatic (E) NK cell–mediated cytotoxicity against activated mouse HSCs (NK:HSC = 10:1; n = 4–6 per group). **(F and G)** Western blot analysis of protein levels of EP3 in hepatic NK cells from CCL4-treated (F) and BDL-treated (G) HA-tagged EP3 transgenic mice. **(H)** Cytotoxicity of NK cells from spleen of EP3$^{-/-}$ mice against activated mouse HSCs (NK:HSC = 10:1; n = 5 per group). **(I)** Cytotoxicity of NK cells from liver of EP3$^{-/-}$ mice against activated mouse HSCs (NK:HSC = 10:1; n = 5 per group). Data are representative of two independent experiments (A–H). Data represent mean ± SEM. Statistical significance was evaluated by Mann–Whitney U tests (A, B, H, and I) and one-way ANOVA followed by Tukey's test for multiple comparisons (C, D, and E). *, P < 0.05; **, P < 0.01; ***, P < 0.001. Source data are available for this figure: SourceData F1.

increased. In fibrotic livers, the proportional shift became more evident: the ratio and number of DP and CD11b SP NK cells were significantly declined, whereas DN and CD27 SP NK cells were markedly increased in EP3$^{F/F}$NKp46^{Cre} mice (Fig. S1, N–S). Interestingly, *EP3* was differently expressed in these NK subtypes, with higher expression in DP NK cells (Fig. S1 T). The liver contains two distinct NK subsets: CD49a^{+}CD49b (DX5)$^{-}$ cells are liver-resident NK cells, and the CD49a^{-}CD49b^{+} cells are conventional NK cells derived from the spleen (Sojka et al., 2014). Indeed, the hepatic DP NK subset was largely CD49a^{-}CD49b^{+} (Fig. S2, A and B). To further explore the functional consequences of EP3 deficiency in NK subsets, we isolated NK cells from each of the four developmental stages of mouse spleen and cocultured them with activated HSCs. Notably, only DP EP3$^{-/-}$ NK cells displayed significantly lower responsiveness to HSC engagement than normal NK cells (Fig. 3, M and N). Both splenic and hepatic DP EP3$^{-/-}$ NK cells had impaired lytic activity against HSCs when stimulated with or without PMA/ionomycin (Fig. 3, O and P). Moreover, adoptive transfer of the NK DP subset from WT spleen to EP3$^{-/-}$ mice (Fig. S3, A and B) rescued the liver injury and fibrosis in CCL4-treated EP3$^{-/-}$ mice (Fig. 3, Q–T), as indicated by decreased hepatic protein levels of fibrogenic markers after DP NK cell injection (Fig. 3, U and V). Thus, the loss of EP3 in NK cells exacerbates LF by impairing the activity of NK DP subsets.

EP3 enhances the adhesion and cytotoxicity of DP NK cells toward activated HSCs through integrin α4–VCAM1 binding

For an in-depth analysis of the molecular alterations mediated by EP3 in NK cells, single-cell RNA sequencing (scRNA-seq) was performed using NK DP cells (Fig. S4 A). A t-distributed stochastic neighbor embedding (t-SNE) analysis revealed five clusters with specific marker genes in DP NK cells (Fig. S4, B and C), which were well aligned in control cells and EP3-deficient NK cells (Fig. 4, A and B). A total of 75 differentially expressed genes (DEGs) comprising 12 upregulated and 63 downregulated genes were identified in EP3-deficient NK cells using the control cells as a reference (fold-change >1.5, P < 0.05). Among the top 30 Gene Ontology (GO) terms (Fig. 4 C), six terms were directly related with NK cell adhesion: heterotypic cell-cell adhesion (biological process [BP]), leukocyte cell-cell adhesion (BP), focal adhesion (cellular component [CC]), cell surface (CC), protein binding (molecular function [MF]), and protein homodimerization (MF). Kyoto Encyclopedia of Genes and Genomes (KEGG) confirmed the adhesion pathway enrichment (Fig. 4 D), and gene set enrichment analysis (GSEA) further revealed that the adhesion signaling pathway was downregulated in EP3-deficient NK cells (Fig. 4 E). We then crossed the adhesion gene set with the top 50 downregulated genes and found five typical adhesion-related genes (*Itga4*, *Tln1*, *Dock2*, *Itgb1*, and *Mhy9*; Fig. 4, F and G), which was also confirmed by qualitative RT-PCR in both

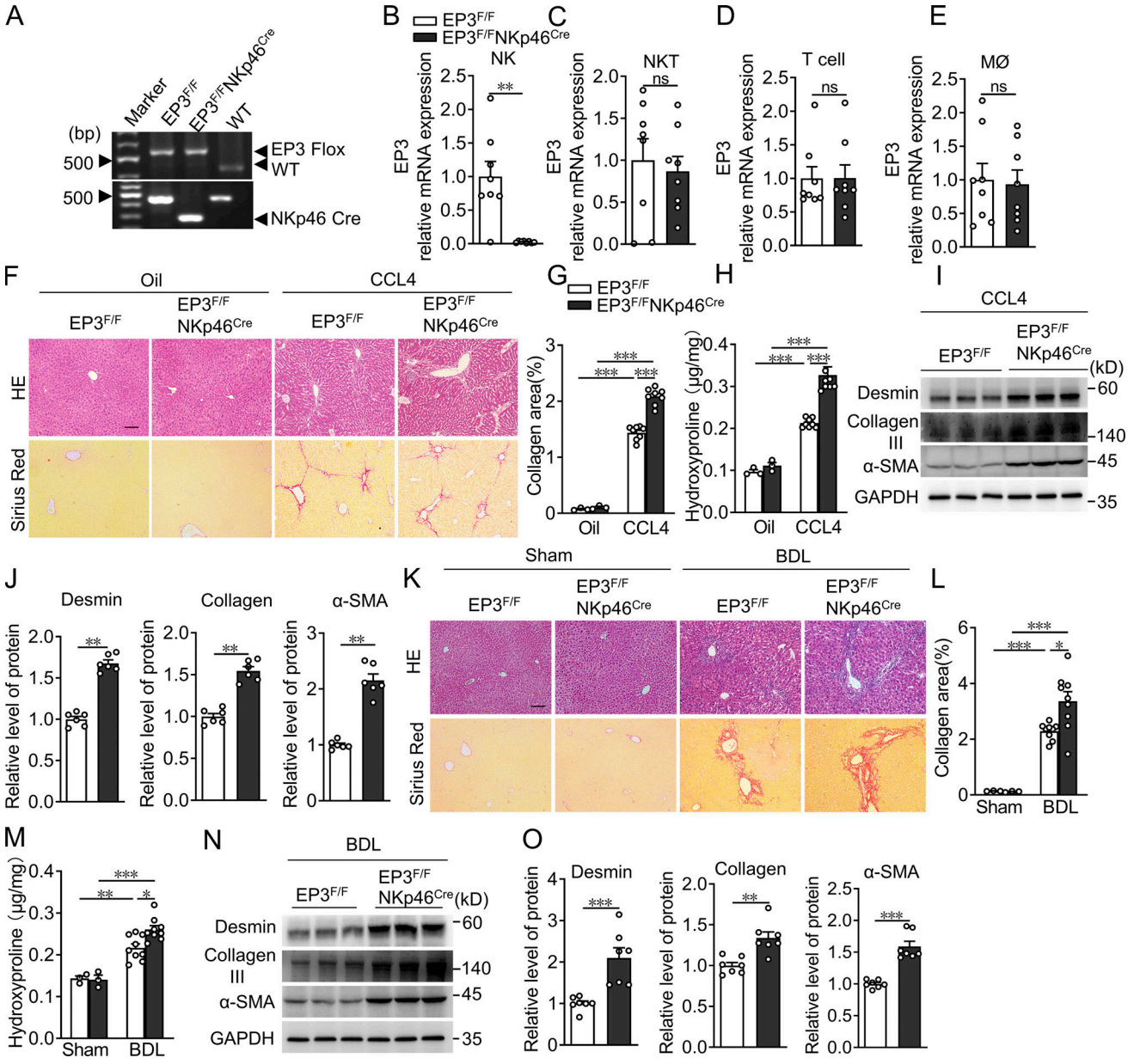

Figure 2. **NK cell–specific deletion of EP3 aggravates CCL4- or BDL-induced LF in mice. (A)** Genotyping of NK cell–specific EP3-deleted mice by PCR of genomic DNA extracted from the tail biopsies. **(B–E)** Quantification of EP3 expression in NK cells (B), NKT cells (C), T cells (D), and macrophages (E) from $EP3^{F/F}$ and $EP3^{F/F}NKp46^{Cre}$ mice (n = 8 per group). **(F)** H&E and Sirius red staining of CCL4-treated liver from $EP3^{F/F}$ and $EP3^{F/F}NKp46^{Cre}$ mice. Scale bars, 100 μm. **(G)** Quantification of Sirius red–stained collagen in F (oil, n = 3 per group; CCL4, n = 8 per group). **(H)** Quantification of hepatic hydroxyproline in CCL4-treated liver from $EP3^{F/F}$ and $EP3^{F/F}NKp46^{Cre}$ mice (oil, n = 3 per group; CCL4, n = 8 per group). **(I)** Western blot analysis of protein levels of α-SMA, collagen III, and desmin in CCL4-treated liver from $EP3^{F/F}$ and $EP3^{F/F}NKp46^{Cre}$ mice. **(J)** Quantification of protein levels in I (n = 6 per group). **(K)** H&E and Sirius red staining of BDL liver from $EP3^{F/F}$ and $EP3^{F/F}NKp46^{Cre}$ mice. Scale bars, 100 μm. **(L)** Quantification of Sirius red–stained collagen in K (oil, n = 3 per group; CCL4, n = 9 per group). **(M)** Quantification of hepatic hydroxyproline in BDL-treated liver from $EP3^{F/F}$ and $EP3^{F/F}NKp46^{Cre}$ mice (oil, n = 3 per group; CCL4, n = 9 per group). **(N)** Western blot analysis of protein levels of α-SMA, collagen III, and desmin in BDL liver from $EP3^{F/F}$ and $EP3^{F/F}NKp46^{Cre}$ mice. **(O)** Quantification of protein levels in N (n = 7 per group). Data are representative of two independent experiments (A–E, F–J, and K–O). Data represent mean ± SEM. Statistical significance was evaluated by Mann–Whitney U test (B, C, D, E, J, and O) and two-way ANOVA followed by Tukey's test for multiple comparisons (G, H, L, and M). *, $P < 0.05$; **, $P < 0.01$; ***, $P < 0.001$. Source data are available for this figure: SourceData F2.

EP3-deficient and EP3-overexpressed NK cells (Fig. 4, H and I). Among them, Itga4 associates with an Itgb1 or Itgb7 subunit to form an integrin that plays an important role in regulating lymphocyte adhesion and migration by binding to ligands such as VCAM-1, MadCAM-1, fibronectin, and osteopontin on target cells (Moreno-Layseca et al., 2019). In HSCs, significantly increased expression of *VCAM1* and *fibronectin* was observed in activated HSCs (Fig. 4 J). Interestingly, EP3 deficiency markedly impaired DP NK cell adhesion to plate-bound VCAM1, but not fibronectin (Fig. 4 K). EP3-deficient NK cells also showed defective lamellipodia formation after VCAM1 engagement, as determined by F-actin staining (Fig. 4, L and M). In contrast,

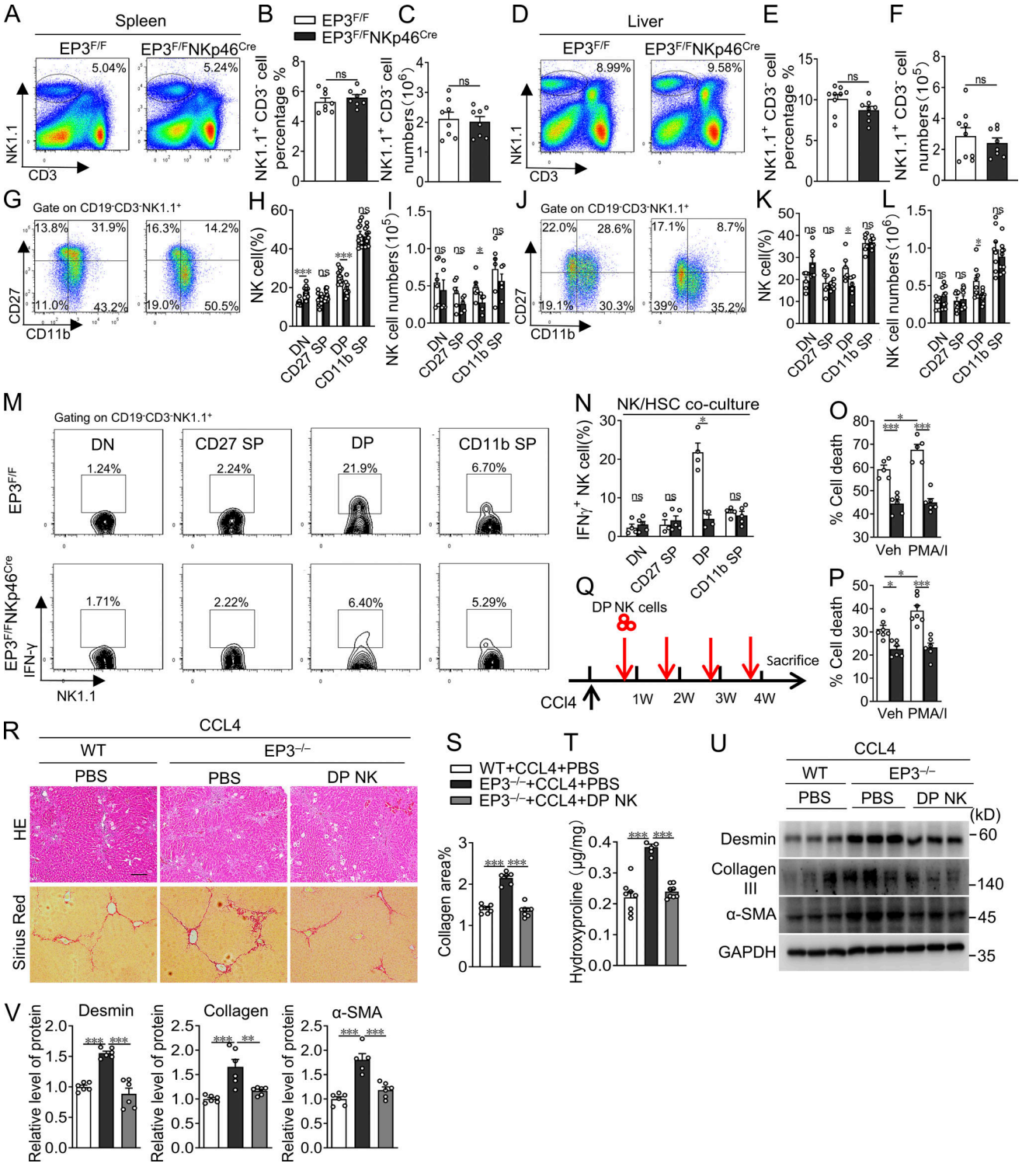

Figure 3. **Adoptive transfer of DP NK cells rescues the aggravated LF induced by CCL4 in EP3-deficient mice. (A–C)** Representative flow cytometric profiles (A), percentages (B), and numbers (C) of splenetic NK1.1$^+$ NK cells from EP3$^{F/F}$ and EP3$^{F/F}$NKp46^{Cre} mice (n = 8 per group). **(D–F)** Representative flow cytometric profiles (D), percentages (E), and numbers (F) of hepatic NK1.1$^+$ NK cells from EP3$^{F/F}$ and EP3$^{F/F}$NKp46^{Cre} mice (n = 8–9 per group). **(G–I)** Representative flow cytometric profiles (G), percentages (H, n = 10 per group), and numbers (I, n = 5–6 per group) of four-stage (DN, CD27 SP, DP, and CD11b SP) development of splenic NK cells (gated as NK1.1$^+$CD3$^-$CD19$^-$) from EP3$^{F/F}$ and EP3$^{F/F}$NKp46^{Cre} mice. **(J–L)** Representative flow cytometric profiles (J), percentages (K, n = 6–7 per group), and numbers (L, n = 7–10 per group) of four-stage development of hepatic NK cells (gated as NK1.1$^+$CD3$^-$CD19$^-$) from EP3$^{F/F}$ and EP3$^{F/F}$NKp46^{Cre} mice. **(M and N)** Representative flow cytometry plots (M) and frequency (N) of IFN-γ–positive NK cells in the four developmental stages from spleens of EP3$^{F/F}$ and EP3$^{F/F}$NKp46^{Cre} mice following stimulation by early activated HSCs (n = 3–5 per group). **(O and P)** Cytotoxicity of DP NK cells from spleens (O) and livers (P) of EP3$^{F/F}$ and EP3$^{F/F}$NKp46^{Cre} mice against activated mouse HSCs (NK cells:HSCs = 10:1) with or without PMA (50 ng/ml)/ionomycin (0.5 μg/ml) prestimulation for 4 h (n = 5–7 per group). **(Q)** Schematic representation of the experimental design for adoptive transfer. **(R)** H&E and Sirius red

staining of CCL4-treated liver from EP3$^{-/-}$ mice after adoptive transfer of DP NK cells. Scale bars, 100 µm. **(S)** Quantification of Sirius red–stained collagen in R (n = 6–8 per group). **(T)** Quantification of hepatic hydroxyproline in CCL4-treated liver from EP3$^{-/-}$ mice after adoptive transfer of DP NK cells (n = 6–8 per group). **(U)** Western blot analysis of protein levels of α-SMA, collagen III, and desmin in CCL4-treated liver from EP3$^{-/-}$ mice after adoptive transfer of DP NK cells. **(V)** Quantification of protein levels in U (n = 5–6 per group). Data are representative of two independent experiments (A–L, M–P, and R–V). Data represent mean ± SEM. Statistical significance was evaluated with Mann–Whitney U test (B, C, E, F, H, I, K, L, and N), two-way ANOVA followed by Tukey's test for multiple comparisons (O and P), and one-way ANOVA followed by Tukey's test for multiple comparisons (S, T, and V). *, P < 0.05; **, P < 0.01; ***, P < 0.001. Source data are available for this figure: SourceData F3.

EP3-overexpressing DP NK cells exhibited stronger VCAM1-dependent adhesion and cytoskeletal remodeling than control cells (Fig. S5, A–C). We observed markedly downregulated *Itga4* expression in hepatic DP NK cells and upregulated *VCAM1* expression in HSCs from CCL4-treated mice. Deletion of EP3 in NK cells suppressed *Itga4* expression in DP NK cells but had no obvious effect on the expression of VCAM1 in activated HSCs (Fig. 4, N and O). Importantly, knockdown of *Itga4* (Fig. 4 P) abrogated the enhanced adhesion of EP3-overexpressed NK cells to VCAM1 (Fig. 4 Q) and attenuated the enhanced attachment and cytotoxicity of EP3-overexpressed DP NK cells toward the activated HSCs (Fig. 4, R and S). Similarly, silencing of VCAM1 in HSCs (Fig. 4 T) prevented the adhesion between EP3-overexpressed DP NK cells and activated HSCs (Fig. 4 U) and subsequently decreased NK cell–mediated lysis of activated HSCs (Fig. 4 V). These results indicated that EP3 promoted adhesion and killing of DP NK cells to activated HSCs through Itag4/VCAM1 binding.

EP3 promotes Itga4 expression of DP NK cells via transcription factor (TF) Spic

To further explore the molecular mechanism underlying EP3-mediated NK cell adhesion, we performed single-cell regulatory network inference and clustering (SCENIC) analysis to identify the key transcription regulators underlying EP3/Itga4 signaling in DP NK cells (Aibar et al., 2017). EP3 deficiency resulted in a significant decline in the activity of Spic and E2f7 and elevation of Bcl11a activity in DP NK cells (Fig. 5 A). GO analysis of the target genes of these TFs using Database for Annotation, Visualization, and Integrated Discovery (DAVID; Huang da et al., 2009) revealed that only Spic-targeted genes were enriched in cell adhesion (Fig. S5, D–F) and the software JASPAR predicted that the promoter regions of the five downregulated adhesion genes (*Itga4*, *Tln1*, *Dock2*, *Itgb1*, and *Mhy9*) also contained putative Spic binding sites (Fig. S5 G). Notably, no significant alteration in Spic mRNA (Fig. 5 B) or protein levels (Fig. 5 C) was observed in EP3-deficient DP NK cells compared with control cells. Indeed, deletion of EP3 reduced (Fig. 5, D–F), while EP3 overexpression increased, the nuclear distribution of Spic in mouse DP NK cells (Fig. S5, H–J). EP3 agonist selectively promoted Spic translocation from the cytosol to the nucleus in normal DP NK cells, but not in EP3-deficient cells (Fig. 5, D–F). Silencing of Spic (Fig. 5 G) abrogated the EP3 overexpression–induced increase in Itga4 expression (Fig. 5 H), enhanced adhesion to VCAM1 (Fig. 5 I), and conjugation to activated HSCs (Fig. 5, J and K). More importantly, Spic deletion in NK cells abolished the antifibrosis effect of EP3 overexpression in NK cells in CCL4-treated mice (Fig. 5, L–P). These data suggest that activation of EP3 attenuated LF by enhancing DP NK cell adhesion to and lysis of activated HSCs by increasing Spic-mediated Itga4 expression in DP NK cells.

Activation of EP3 strengthens Itga4-VCAM1 adhesion of human NK cells via Spic

It has been suggested that murine CD27^{+}CD11b$^{-/+}$ NK cells resemble human CD56^{bright} NK cells (Crinier et al., 2018), including NK-92MI cells, a human NK cell line (Ma et al., 2020). Similar to mouse DP NK cells, NK-92MI cells also expressed *EP3* and showed impaired cytotoxicity against activated HSCs upon EP3 inhibitor treatment in a dose-dependent manner (Fig. 6, A–C). EP3 agonist enhanced, whereas EP3 inhibitor reduced, adhesion to VCAM1 (Fig. 6 D) and cytosol-nuclear translocation of Spic (Fig. 6 E), as well as Itga4 expression in NK-92MI cells (Fig. 6 F). Knockdown of Spic (Fig. 6 G) also abrogated the EP3 agonist–induced increase in Itga4 expression and enhanced adhesion to VCAM1 (Fig. 6, H and I). Furthermore, NK cells isolated from peripheral blood mononuclear cells were dramatically decreased in patients with alcoholic liver cirrhosis (ALC) compared with those from healthy controls (Fig.6, J–L). *EP3* expression was also downregulated in NK cells from ALC patients compared with healthy controls (Fig. 6 M). EP3 agonist promoted *Itga4* expression (Fig. 6 N) and enhanced the adhesion and cytotoxicity of NK cells against HSCs in both healthy controls and ALC patients, although these NK functions were significantly impaired in ALC patients compared with those in healthy controls (Fig. 6, O and P), suggesting that EP3 is an important regulator of human NK function in LF.

EP3 enhances Spic-mediated Itga4 expression in NK cells through Ca^{2+}/PKC signaling pathway

As a G protein–coupled receptor, EP3 is mainly coupled to $G_{\alpha i}$ to reduce intracellular cAMP levels, but in particular cell types, EP3 might couple with different G proteins, such as $G_{\alpha s}$ or $G_{\alpha q}$, to stimulate cAMP production or mobilize cytosolic Ca^{2+}, respectively (Biringer, 2021). Notably, only the phospholipase C inhibitor U73122, which reduces intracellular Ca^{2+} influx, significantly prevented EP3 agonist-induced cytosol-nuclear translocation of Spic in NK-92MI cells (Fig. 7 A). Consistently, EP3-deficient NK cells exhibited impaired intracellular Ca^{2+} influx upon EP3 agonist treatment (Fig. 7 B), and U73122 pretreatment abolished EP3 agonist-triggered Ca^{2+} influx in normal mouse DP NK cells and NK-92MI cells (Fig. 7, B and C). As a second messenger, Ca^{2+} exerts multiple cellular functions mainly through Ca^{2+}-dependent protein kinases, such as CaM kinase and PKC. By aligning the Spic protein amino acid sequences of different species, we identified a conserved (R/K; R/K)Xp(S/T)X(R/X) motif for PKC phosphorylation at Thr191 (Fig. 7 D) using NetPhos 3.1, Scansite 4.0, and PhoScan.

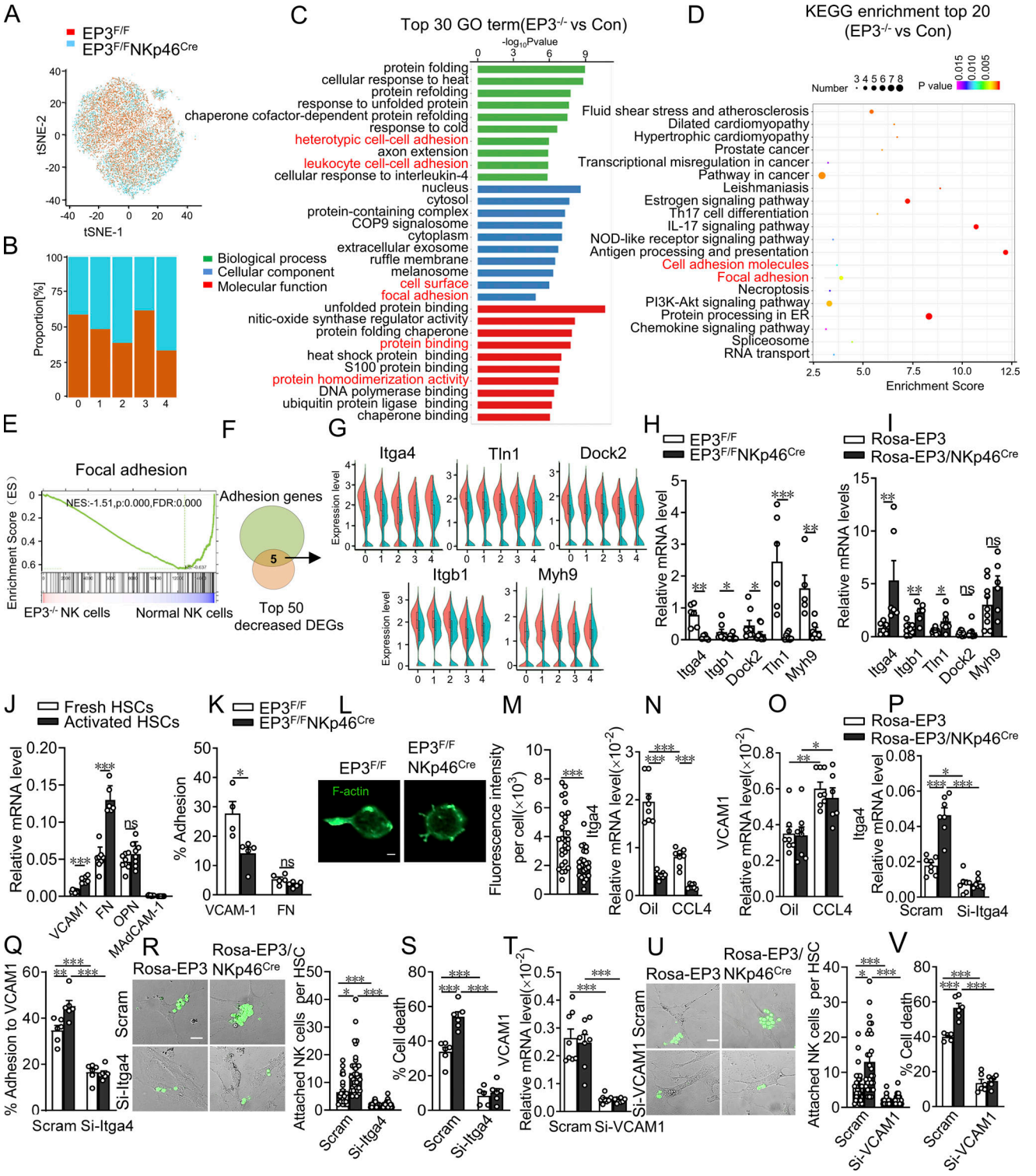

Figure 4. **Activation of EP3 promotes DP NK cell adhesion to activated HSCs through Itga4-VCAM1 binding. (A)** t-SNE plots of control and EP3-deficient DP NK cells, determined by Seurat. **(B)** Percentages of cells from each cluster in each sample. **(C)** Top 30 most enriched GO terms (BP, CC, MF) associated with DEGs. **(D)** Top 20 most enriched KEGG pathways associated with DEGs ($EP3^{F/F}NKp46^{Cre}$ vs. $EP3^{F/F}$). **(E)** GSEA analysis of focal adhesion pathway genes altered by EP3 deletion ($EP3^{F/F}NKp46^{Cre}$ vs. $EP3^{F/F}$). **(F)** Adhesion-related genes in TOP50 DEGs. Green circle, adhesion genes; brown circle, top 50 downregulated DEGs. **(G)** Violin plots displaying the expression profile of selected adhesion-related genes across the clusters in control and EP3-deficient DP NK cells. **(H)** Relative mRNA levels of selected adhesion related genes in control and EP3-deficient DP NK cells (n = 5–9 per group). **(I)** Relative mRNA levels of selected adhesion related genes in control and EP3-overexpressed DP NK cells (n = 6–9 per group). **(J)** Relative mRNA levels of *Itga4* binding ligand in activated HSCs (n = 6–8 per group). **(K)** Ratio of cell adhesion to plate-bound VCAM1 and fibronectin in control and EP3-deficient DP NK cells (n = 4–5 per group). **(L)** Immunofluorescence images of F-actin–stained with phalloidin in control and EP3-deficient DP NK cells. Scale bars, 2 µm. **(M)** Qualification of the density of F-actin filaments in L (n = 24–27 per group). **(N)** Relative mRNA levels of *Itga4* in hepatic DP NK cells from $EP3^{F/F}$ and $EP3^{F/F}NKp46^{Cre}$ mice with CCL4 treatment (n = 8

per group). **(O)** Relative mRNA levels of *VCAM1* in HSCs from $EP3^{F/F}$ and $EP3^{F/F}NKp46^{Cre}$ mice with CCL4 treatment (n = 6–8 per group). **(P)** Knockdown efficiency of siRNA of *Itga4* in DP NK cells (n = 7–8 per group). **(Q)** Ratio of cell adhesion to plate-bound VCAM1 in control and EP3-overexpressed DP NK cells after knockdown of *Itga4* in NK cells (n = 6 per group). **(R)** Representative immunofluorescence images and ratio of adhesion of EP3-overexpressed DP NK cells to activated HSCs after knockdown of Itga4 in NK cells (n = 27–34 per group). Scale bars, 20 µm. **(S)** Cytotoxicity of EP3-overexpressed DP NK cells against activated mouse HSCs after knockdown of *Itga4* in NK cells (n = 5–6 per group). **(T)** Knockdown efficiency of siRNA of *VCAM1* in activated HSCs (n = 8 per group). **(U)** Representative immunofluorescence images and ratio of adhesion of EP3-overexpressed DP NK cells to activated HSCs after knockdown of VCAM1 in HSCs (n = 28–38 per group). Scale bars, 20 µm. **(V)** Cytotoxicity of EP3-overexpressed DP NK cells against activated mouse HSCs after knockdown of *VCAM1* in HSCs (n = 5–6 per group). Data are representative of two independent experiments (H–V). Data represent mean ± SEM. Statistical significance was evaluated with Mann–Whitney U test (H–K and M), two-way ANOVA followed by Tukey's test for multiple comparisons (N–P, Q, S, T, and V), and Kruskal–Wallis tests followed by Dunn's test for multiple comparisons (R and U). *, P < 0.05; **, P < 0.01; ***, P < 0.001.

Activation of PKC induced the phosphorylation of the PKC substrate motif in HA-tagged WT Spic and T166A mutant (a non-PKC phosphorylation site) but not the T191A mutant in transfected 293T cells, while inhibition of PKC blocked PKC agonist–induced phosphorylation of Spic (Fig. 7 E), suggesting that PKC may directly phosphorylate Spic on T191 in NK cells. Furthermore, EP3 agonist-induced Spic T191 phosphorylation was also prevented by PKC inhibition in 293T cells, and blockage of intracellular Ca^{2+} transients with U73122 abolished Spic T191 phosphorylation by EP3 agonist treatment (Fig. 7 F). Finally, inhibition of Ca^{2+} influx and PKC activity attenuated the EP3 agonist–induced increase in Itga4 expression by blocking cytosol-nuclear translocation of Spic in NK-92MI cells (Fig. 7 G). Thus, activation of EP3 upregulates *Itga4* expression by promoting cytosol-nuclear translocation of Spic through Ca^{2+}/PKC-dependent T191 phosphorylation of Spic in NK cells, which may enhance the adhesion and cytotoxicity of NK cells against activated HSCs (Fig. 7 H).

Activation of EP3 attenuates CCL4-induced LF in mice

Finally, we investigated whether activation of EP3 could alleviate LF. 1 wk after CCL4 induction, mice were injected with EP3 agonist sulprostone (i.p., 80 µg/kg/d) for another 2 wk with CCL4 treatment (Fig. 8 A). We found that treatment of sulprostone prevented the loss of DP NK cells due to CCL4 challenge but had no obvious effect on the EP3-deficient DP NK cells (Fig. 8, B–D). Sulprostone also markedly attenuated CCL4-induced liver injury and reduced collagen deposition in WT mice, not in EP3 mutant mice (Fig. 8, E–I). Thus, targeting EP3 may constitute a therapeutic strategy for LF.

Discussion

In this study, we showed that deletion of EP3 aggravated LF, whereas EP3 overexpression in NK cells or pharmacological activation of EP3 attenuated LF in mice. EP3 deficiency suppressed the adhesion of the DP NK subset to activated HSCs through disruption of Itga4–VCAM1 interaction and impaired its killing capability. Activation of EP3 promoted Itga4 expression through Ca^{2+}/PKC-dependent Spic phosphorylation in NK cells. Thus, EP3 is essential for NK cell adhesion and removal of active HSCs during LF.

Accumulating evidence has shown that PGE_2 is a potent physiological suppressor of LF. Treatment with PGE_2 confers a liver-protective effect against LF in animals by directly inhibiting HSC activation (Hui et al., 2004; Schippers et al., 2017). Attenuation of PGE_2 production by mPGES-1 ablation exacerbates the inflammatory response and hepatic fibrosis in nonalcoholic steatohepatitis mice (Henkel et al., 2018). In agreement with the antifibrotic effects of PGE_2, we found that either global deletion or the conditional ablation of the PGE_2 receptor EP3 in NK cells aggravated injury-induced LF in mice, whereas EP3 overexpression in NK cells or pharmacological activation of EP3 alleviated LF in mice. Indeed, $EP3^{-/-}$ mice showed delayed liver repair after hepatic ischemia-reperfusion injury compared with WT mice (Nakamoto et al., 2020). Therefore, EP3 inhibition may serve as a therapeutic target for the management of LF.

Selective activation of PGE_2 receptor EP2 or EP4 inhibits NK cell cytotoxicity against tumor cells (Bonavita et al., 2020). In contrast, activation of EP1/EP3 specifically promotes NK cell migration (Holt et al., 2011), indicating that the effect of PGE_2 on NK cells may functionally differ depending on different EP receptors and NK subsets. We found that activation of EP3 enhanced DP NK cell adhesion and cytotoxicity in activated HSCs. Similarly, PGE_2 was reported to promote adhesion between the $CD25^+CD54^+$ NK subset and tumor cells and augment tumor cell lysis (Chen et al., 2021). PGE_2 also strengthens cell matrix adhesion in cancer cells (Massoumi et al., 2003; Mayoral et al., 2005) and facilitates hematopoietic stem cell homing after transplantation (Hoggatt et al., 2009). Deletion of EP3 abolishes PGE_2-induced adhesion of mast cells to the matrix (Sakanaka et al., 2008). As an intermediate mature NK subset, DP cells exhibit cytotoxicity by producing high levels of cytokines (Fu et al., 2011). Dynamic shift of hepatic NK cells to immature or highly cytolytic subsets promotes hepatic tumor progression (Zhang et al., 2017) and liver injury (Gomez-Santos et al., 2012), respectively. Loss of EP3 in NK cells resulted in increased immature NK cells and reduced DP NK cells in mice, which may accelerate the process of LF. We found that adoptive transfer of DP NK cells markedly improved LF in CCL4-treated EP3-deficient mice. Thus, the PGE_2/EP3 axis mediates the anti-hepatic fibrosis effect by governing DP NK cell function.

Itga4/VCAM1 interaction plays a vital role in cell–cell adhesion and migration, such as leukocyte adhesion to the endothelium and homing of hematopoietic stem and progenitor cells (Osborn et al., 1992; Ramirez et al., 2009). Itga4/VCAM1 binding is essential for NK cell adhesion and transmigration across the endothelium (Allavena et al., 1996; Melder et al., 1996). In activated HSCs, *VCAM1* expression is also significantly upregulated (Fujita and Narumiya, 2016). During the progression of LF, activated HSCs are no longer shielded from immune cells by

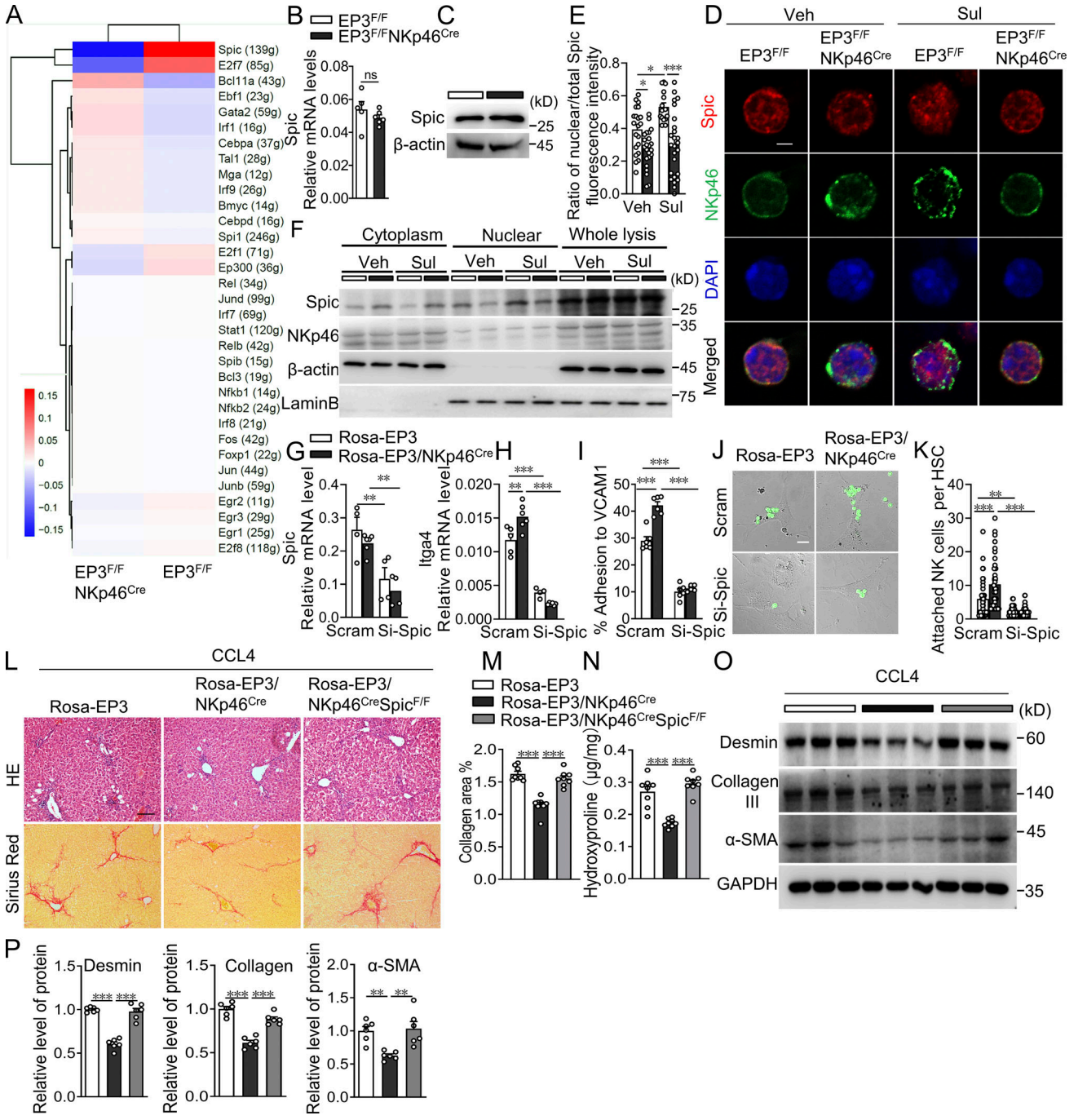

Figure 5. **TF Spic is required for EP3-mediated Itga4 expression in DP NK cells. (A)** Inferred TFs in control and EP3-deficient DP NK cells by SCENIC analysis. **(B)** Relative mRNA level of *Spic* in control and EP3-deficient DP NK cells (n = 5–6 per group). **(C)** Western blot assay of Spic in control and EP3-deficient DP NK cells. **(D and E)** Representative immunofluorescence images (D) and ratio (E) of nuclear distribution of Spic in EP3 agonist-treated DP NK cells (n = 15–25 per group). Scale bars, 2 μm. **(F)** Western blot assay of cytosol-nuclear distribution of Spic in EP3 agonist-treated DP NK cells. **(G)** Knockdown efficiency of siRNA of *Spic* in control and EP3-overexpressed DP NK cells (n = 4–6 per group). **(H)** Relative mRNA level of *Itga4* in control and EP3-overexpressed DP NK cells after knockdown of *Spic* in NK cells (n = 4–6 per group). **(I)** Ratio of adhesion of EP3-overexpressed DP NK cells to VCAM1 after knockdown of Spic in NK cells (n = 5–6 per group). **(J and K)** Representative immunofluorescence images (J) and ratio (K) of adhesion of EP3-overexpressed DP NK cells to activated HSCs after knockdown of Spic in NK cells (n = 35–40 per group). Scale bars, 20 μm. **(L)** H&E and Sirius red staining of CCL4-treated liver from Rosa-EP3/NKp46^{Cre} and Rosa-EP3/NKp46^{Cre}Spic$^{F/F}$ mice. Scale bars, 100 μm. **(M)** Quantification of Sirius red–stained collagen in L (n = 8 per group). **(N)** Quantification of hepatic hydroxyproline in CCL4-treated liver from Rosa-EP3/NKp46^{Cre} and Rosa-EP3/NKp46^{Cre}Spic$^{F/F}$ mice (n = 8 per group). **(O)** Western blot analysis of protein levels of α-SMA, collagen III, and desmin in CCL4-treated liver from Rosa-EP3/NKp46^{Cre} and Rosa-EP3/NKp46^{Cre}Spic$^{F/F}$ mice. **(P)** Quantification of protein levels in O (n = 6 per group). Data are representative of two independent experiments (B–P). Data represent mean ± SEM. Statistical significance was evaluated with Mann–Whitney U test (B), two-way ANOVA followed by Tukey's test for multiple comparisons (E, G–I, and K), and one-way ANOVA followed by Tukey's test for multiple comparisons (M, N, and P). *, P < 0.05; **, P < 0.01; ***, P < 0.001. Source data are available for this figure: SourceData F5.

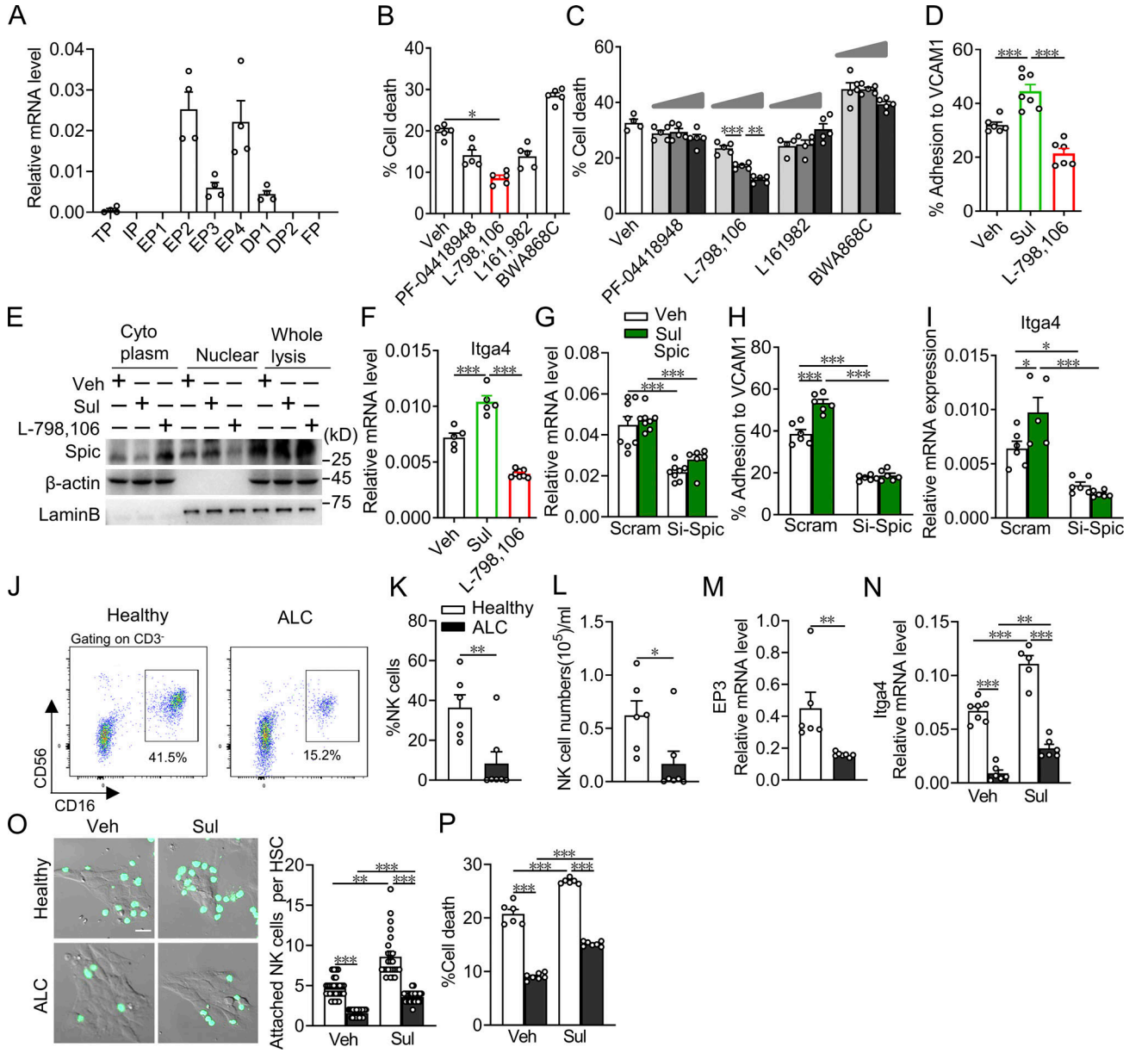

Figure 6. **Activation of EP3 enhances human NK-92MI cell adhesion to VCAM1 through Spic. (A)** Expression profile of PG receptors in human NK cells (NK-92MI; *n* = 4 per group). **(B)** Cytotoxicity toward LX-2 cells (human HSC cell line) was analyzed in NK-92MI cells (NK-92MI:LX2 = 10:1) after treatment with inhibitors of PG receptors (PF-04418948 for EP2; L-798,106 for EP3; L161,982 for EP4; and BW A868C for DP1; *n* = 5 per group). **(C)** Dose-dependent effect of PG receptor inhibitor on NK-92MI cell–mediated cytotoxicity toward LX-2 cells (NK-92MI:LX2 = 10:1; *n* = 4–5 per group). **(D)** Ratio of adhesion of NK-92MI cells to VCAM1 after treatment with sulprostone or L-798,106 (*n* = 6–7 per group). **(E)** Western blot assay of cytosol-nuclear distribution of Spic in NK-92MI cells after treatment with sulprostone or L-798,106. **(F)** Relative mRNA levels of *Itga4* in NK-92MI cells after treatment with sulprostone or L-798,106 (*n* = 5–8 per group). **(G)** *Spic* expression in NK-92MI cells after treatment with siRNA (*n* = 6–8 per group). **(H)** Effect of *Spic* silencing on adhesion of NK-92MI cells to VCAM1 with sulprostone treatment (*n* = 6 per group). **(I)** Effect of *Spic* silencing on mRNA levels of *Itga4* in NK-92MI cells treated with sulprostone (*n* = 5–6 per group). **(J–L)** Representative flow cytometric profiles (J), percentages (K), and cell numbers (L) of NK cells from peripheral blood mononuclear cells of healthy controls and patients with ALC (*n* = 6–7 per group). **(M)** Relative mRNA levels of *EP3* in blood NK cells from healthy controls and patients (*n* = 6–7 per group). **(N)** Relative mRNA levels of *Itga4* in blood NK cells from healthy controls and patients with sulprostone treatment (*n* = 5–7 per group). **(O)** Representative immunofluorescence images and ratio of adhesion of blood NK cells from healthy controls and patients to LX-2 cells with sulprostone treatment (*n* = 25–31 per group). Scale bars, 20 µm. **(P)** Cytotoxicity of blood NK cells from healthy controls and patients against LX-2 cells with sulprostone treatment (*n* = 6–7 per group). Data are representative of two independent experiments (A–I). Data represent mean ± SEM. Statistical significance was evaluated with Kruskal–Wallis tests followed by Dunn's test for multiple comparisons (B and O), one-way ANOVA followed by Tukey's test for multiple comparisons (C, D, and F), Mann–Whitney *U* tests (K–M), and two-way ANOVA followed by Tukey's test for multiple comparisons (G–I, N, and P). *, P < 0.05; **, P < 0.01; ***, P < 0.001. Source data are available for this figure: SourceData F6.

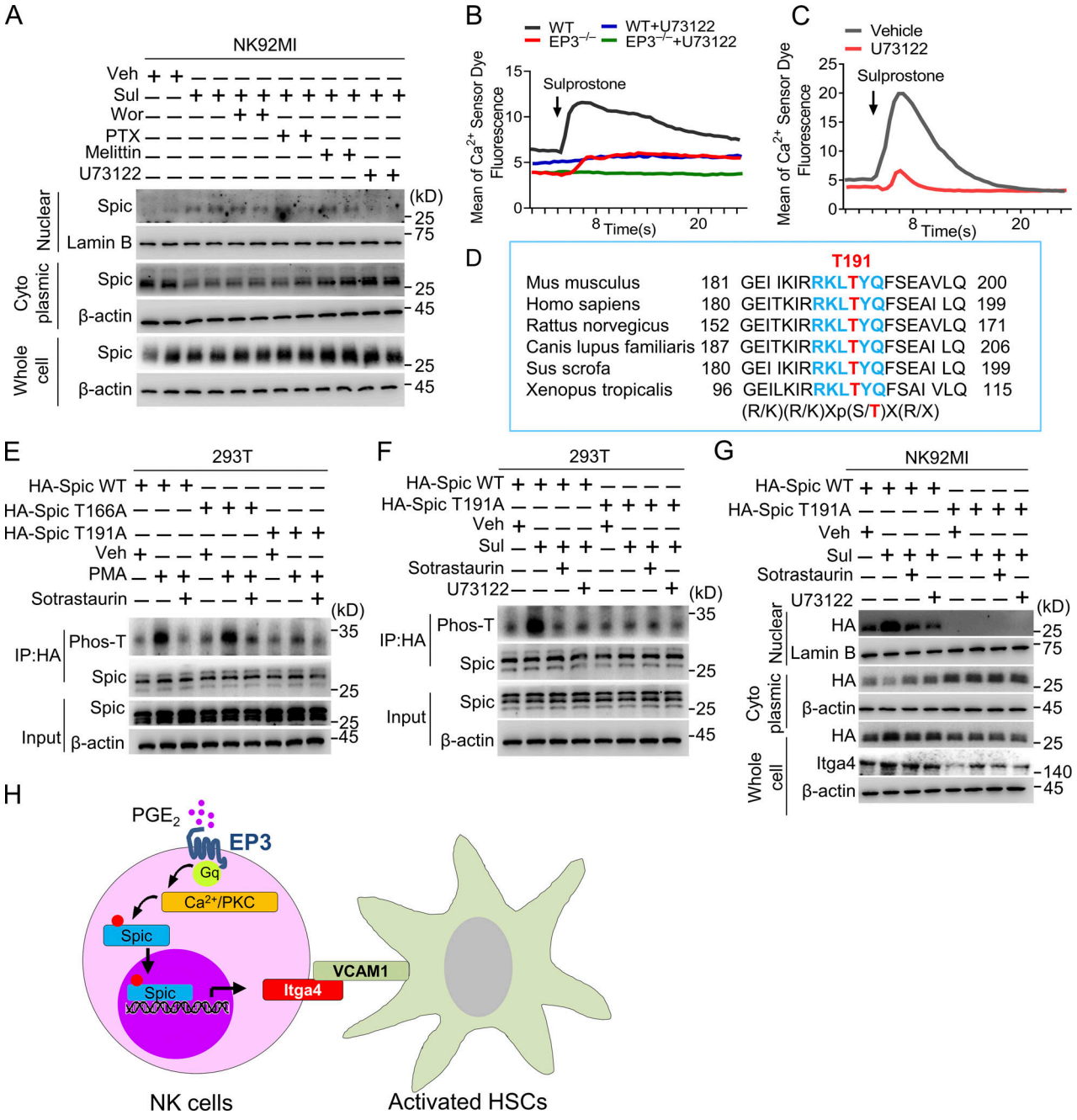

Figure 7. **EP3 promotes *Itga4* expression in NK cells via Ca^{2+}/PKC/Spic signaling pathway. (A)** Effect of Wortmannin (Wor), Pertussis toxin (PTX), U73122, and Melittin on cytosol-nuclear distribution of Spic in NK-92MI cells after treatment with sulprostone. **(B)** Effect of U73122 on Ca^{2+} influx in control and EP3-deficient DP NK cells upon sulprostone treatment. **(C)** Effect of U73122 on Ca^{2+} influx in NK-92MI cells with sulprostone treatment. **(D)** Alignment of residues surrounding Spic T191 (red) with the known PKC substrate phosphorylation motif (blue) from various species. **(E)** Immunoprecipitation analysis of phospho-Spic T191 in lysates of NK-92MI cells transfected with plasmids encoding HA-tagged Spic WT, T166A, or T191A after treatment of PKC inhibitor sotrastaurin and stimulation of PMA. **(F)** Immunoprecipitation analysis of phospho-Spic T191 in lysates of NK-92MI cells transfected with plasmids encoding HA-tagged Spic WT or T191A after treatment with PKC inhibitor sotrastaurin and stimulation by sulprostone. **(G)** Western blot assay of cytosol-nuclear distribution of Spic in NK-92MI cells transfected with plasmids encoding HA-tagged Spic WT or T191A after stimulation of sulprostone and treatment of sotrastaurin or U73122. **(H)** Schematic illustration of EP3-mediated Itga4 expression in NK cells through Ca^{2+}/PKC/Spic signaling. Data are representative of two independent experiments (A–C and E–G). Source data are available for this figure: SourceData F7.

endothelial cells after damage induction and are in direct contact with NK cells (Fasbender et al., 2016). We identified that EP3 activation facilitates Itga4/VCAM1 binding for DP NK cell adhesion to and killing of activated HSCs. Indeed, PGE_2 enhances integrin-mediated human umbilical vein endothelial cell adhesion and spreading (Dormond et al., 2002; Dormond et al., 2001). Blockage of Itga4 prevents NK cell infiltration into the mouse liver (Fogler et al., 1996). Serum levels of VCAM1 are positively

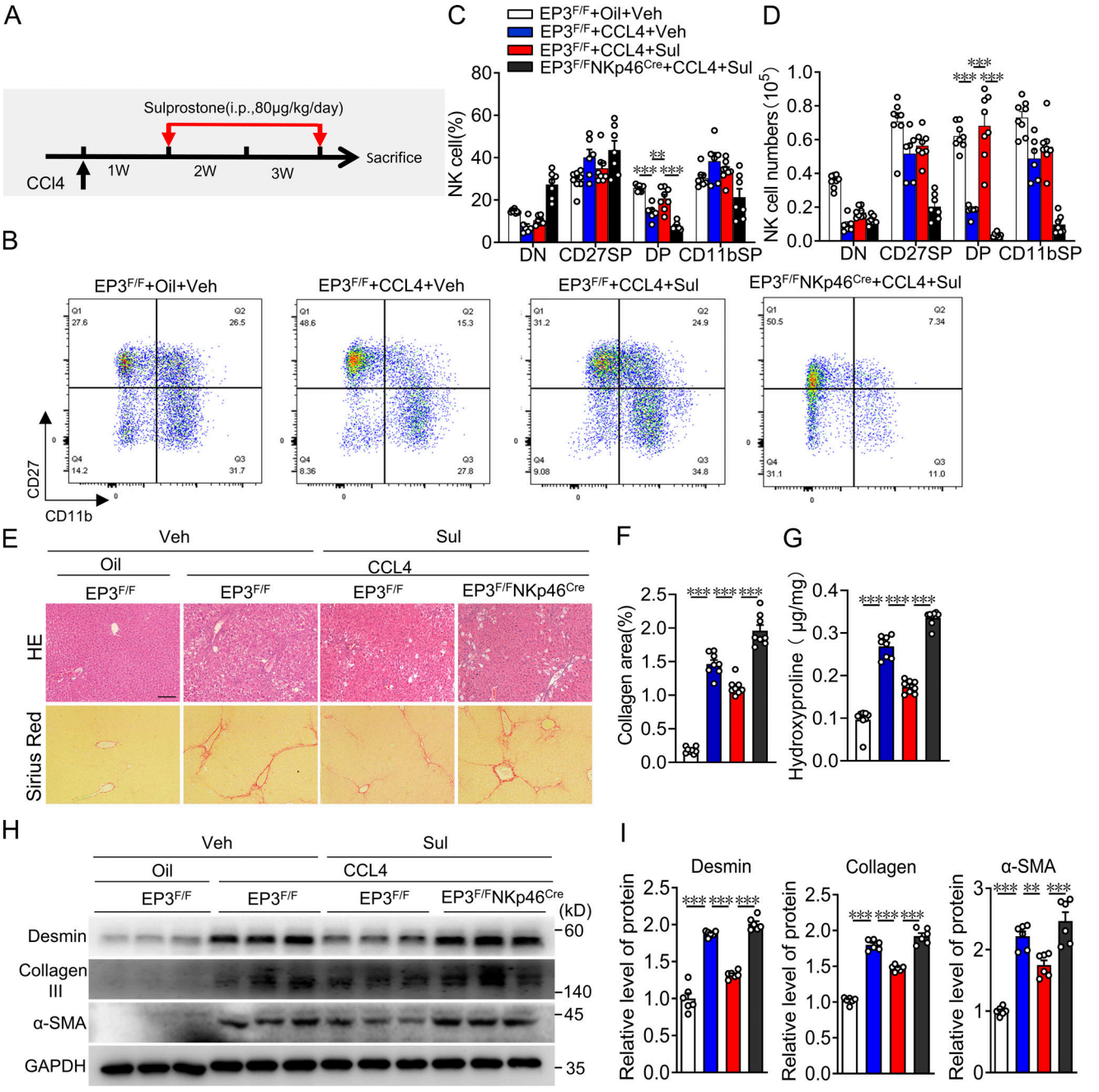

Figure 8. **Treatment of EP3 agonist alleviates CCL4-induced LF in mice. (A)** Protocol for administration of EP3 agonist sulprostone to CCL4-challenged mice. W, week. **(B–D)** Representative flow cytometric profiles (B), percentages (C), and numbers (D) of four-stage development of hepatic NK cells from CCL4-challenged mice with or without sulprostone treatment (n = 6–8 per group). **(E)** H&E and Sirius red staining of liver from CCL4-challenged mice with (Sul) or without (Veh) sulprostone treatment. Scale bars, 100 μm. **(F)** Quantification of Sirius red–stained collagen in E (n = 8 per group). **(G)** Quantification of hepatic hydroxyproline in CCL4-treated liver from CCL4-challenged mice with or without sulprostone treatment (n = 8 per group). **(H)** Western blot analysis of hepatic protein levels of α-SMA, collagen III, and desmin in CCL4-challenged mice with or without sulprostone treatment. **(I)** Quantification of protein levels in H (n = 6 per group). Data are representative of two independent experiments (B–D and E–I). Data represent mean ± SEM. Statistical significance was evaluated with one-way ANOVA followed by Tukey's test for multiple comparisons (C, D, F, G, and I). **, P < 0.01; ***, P < 0.001. Source data are available for this figure: SourceData F8.

associated with the severity of hepatic fibrosis and poor prognosis in patients with liver cirrhosis (Buck et al., 2014; Solé et al., 2016). Pharmacological inhibition or antibody neutralization of VCAM1 attenuated nonalcoholic steatohepatitis in mice (Furuta et al., 2021).

Spic, a PU.1-related TF, controls the development of red pulp macrophages (Kohyama et al., 2009), B cells (Laramee et al., 2020), and osteoclasts (Go et al., 2020), partially by upregulation of adhesion genes such as integrin αM and αD (Haldar et al., 2014; Okreglicka et al., 2021). Deletion of EP3 caused functional

defects in adhesion and cytolysis in DP NK cells through reducing the activity of Spic, which also interrupts development of NK cells (Kohyama et al., 2009). EP3 activation upregulated *Itga4* expression in NK cells by promoting translocation of cytosolic Spic to the nucleus through Ca^{2+}/PKC-dependent phosphorylation of Spic at T191. Consistent with our observations, PGE_2 also promotes tumor cell invasion through PGE_2-mediated integrin upregulation (Bai et al., 2014; Liu et al., 2010; Pan et al., 2016).

In summary, we have demonstrated that EP3-mediated NK cell activation conferred protection against injury-induced LF in mice through PKC/Spic/Itga4 signaling. Activation of EP3 in NK cells could be a therapeutic strategy for combating LF.

Materials and methods

Human study

Human blood samples were obtained from patients with ALC in the Department of Gastroenterology and Hepatology of Tianjin Medical University General Hospital. The study conformed to the ethical guidelines of the World Medical Association Declaration of Helsinki and was approved by the Ethical Committee of Tianjin Medical University General Hospital (institutional review board no. IRB2022-KY-005). Patients who had excessive alcohol consumption (>40 g/d for men and 20 g/d for women) were included in the study. ALC was diagnosed in accordance with the guidelines of prevention and treatment for alcoholic liver disease of China (Li and Fan, 2019). Patients with other causes of chronic liver disease such as hepatophilic virus infection (hepatitis B virus and hepatitis C virus) and drug- or toxin-induced liver damage and autoimmune liver disease, or with severe liver and kidney insufficiency, cardiovascular or cerebrovascular diseases, or malignant tumors, were excluded from the study. Healthy volunteers were recruited from staff of the Tianjin Medical University. All participants provided written informed consent. The clinical characteristics of the subjects are listed in Table S1.

Animals

8–10-wk-old male mice were used in all the experiments. WT mice (C57BL/6J) were purchased from Beijing Vital River Laboratory Animal Technology Co. Rosa-RFP mice were obtained from Prof. Bin Zhou (University of Chinese Academy of Sciences, Beijing, China; Liu et al., 2016). $EP3^{-/-}$, $EP3^{F/F}$, and $NKp46^{Cre}$ mice were bred in our lab (Lazarus et al., 2007; Tang et al., 2017; Yu et al., 2021). Rosa-EP3 mice were generated by Cyagen Biosciences Inc.(#KICMS171208AN1) using CRISPR/Cas-mediated genome engineering. $Spic^{F/F}$ mice were purchased from Gem-Pharmatech Co. (strain no. T009698). HA-EP3 mice were generated using CRISPR/Cas9 strategy by the Center for Excellence in Molecular Cell Science of Chinese Academy of Sciences (genome-tagging project code 19000510). $NKp46^{Cre}$ mice were crossed with $EP3^{F/F}$ or Rosa-EP3 mice to generate $EP3^{F/F}NKp46^{Cre}$ or Rosa-EP3/$NKp46^{Cre}$ mice, respectively. Rosa-EP3/$NKp46^{Cre}Spic^{F/F}$ mice were obtained by crossing Rosa-EP3/$NKp46^{Cre}$ with $Spic^{F/F}$ mice. All mice were maintained on a C57BL/6 genetic background. Mice were maintained in the specific pathogen–free animal laboratory of Tianjin Medical University in an environment with controlled temperature (22 ± 1°C) and relative humidity (50 ± 5%) on a 12:12-h light/dark cycle, with free access to sterile food and water. All animal experiments were performed in accordance with the approval of the Laboratory Animal Management and Use Committee of Tianjin Medical University.

Reagents

We purchased SC-51322 (#10010744), PF-04418948 (#15016), L-798,106 (#11129), sulprostone (#14765), L161982 (#10011565), SQ29548 (#19025), CAY10441 (#10005186), AL8810 (#16735), and BW A868C (#12060) from Cayman Chemical. CCL4 (#1601168), ionomycin (#I3909), and mineral oil (#330779) were purchased from Sigma-Aldrich, and 5(6)-carboxyfluorescein diacetate succinimidyl ester (CFDA-SE) was purchased from DOJINDO Molecular Technology (#150347-59-4). Pertussis toxin was purchased from List Biological Laboratories (#180), and U73122 (#HY-13419), PMA (#HY-18739), melittin (#HY-P0233), and wortmannin (#HY-10197) were purchased from MedChemExpress. Sotrastaurin was purchased from Selleckchem (#S2791). Phalloidin was purchased from Abcam (#ab176753). Percoll was purchased from Solarbio Science & Technology Co. (#P8370).

Rodent models of LF

Hepatic fibrosis in mice was induced by i.p. injection of 2 ml/kg body weight of 25% CCL4 dissolved in mineral oil, twice a week for up to 4 wk (Mitra et al., 2014). BDL was performed as described previously (Kahraman et al., 2008). To identify pharmacological effect of EP3 agonist, mice were i.p. treated with sulprostone (80 µg/kg/d) after 1 wk of CCL4 injection during 2 wk of CCL4 treatment (Chen et al., 2017a; Choi et al., 2021). The mice subjected to BDL were anesthetized with isoflurane, followed by midline laparotomy. The common bile duct was ligated twice with 6–0 silk sutures and cut between the ligations. Sham-operated mice underwent laparotomy without BDL. The mice that received BDL or sham operation were sacrificed 15 d later.

Adoptive transfer of DP NK cells

WT DP NK cells from mouse spleens were isolated using flow cytometry. Adoptive transfer was performed as previously reported (Mitra et al., 2014). Isolated WT DP NK cells (~1×10^5) were injected through the tail vein into $EP3^{-/-}$ mice once a week for 4 wk during CCL4 challenge. Successful delivery was confirmed by flow cytometry using NK cells from the RFP mice.

Plasmid construction

Mouse WT Spic cDNA with an HA tag added to the extracellular C-terminus was amplified by RT-PCR, and T166A and T191A Spic mutants were obtained by site-directed mutagenesis before they were cloned into the pcDNA3.1 vector (Promega) using T4 DNA Ligase (Takara). Correct insertion of DNA fragments was confirmed by sequencing.

Cell isolation, culturing, and transfection

Mouse liver HSCs were isolated by in situ collagenase perfusion and differential centrifugation by OptiPrep (#D1556; Sigma-

Aldrich) density gradients, as described previously, with some modifications (Mederacke et al., 2015). The purity of HSCs was >90% as determined by light microscopy examination of typical lipid droplet appearance. HSCs were cultured in RPMI 1640 with 10% FBS (#10091155; Gibco; Thermo Fisher Scientific) and 1% penicillin-streptomycin (PS; Invitrogen) on plastic plates for 5 d to activate themselves spontaneously (early activated HSCs). The human HSC line LX-2 (#SCC064; Sigma-Aldrich) was maintained in DMEM with 10% FBS and 1% PS. Mouse spleen single-cell suspension was obtained by pressing the spleen through a strainer. A single-cell suspension from mouse liver was created by 0.01% collagenase I and Percoll density gradient centrifugation (Suh et al., 2012). NK cells were isolated from single-cell suspensions using an EasySep Mouse NK Cell Isolation Kit (#19855; Stem Cell). The primary NK cells were maintained in α-MEM with 10% FBS, 10% horse serum (#26050088; Gibco), 0.1 mM β-mercaptoethanol (#M8211; Solarbio), 0.02 mM folic acid (#F8758; Sigma-Aldrich), 0.2 mM inositol (#I7508; Sigma-Aldrich), 10 ng/ml mouse recombinant IL-2 (#212-12; Peprotech), and 1% PS. To detect intracellular IFN-γ, GolgiStop (0.2 µl per well; BD Biosciences) was added to the NK cells in the last 5 h of culturing. The human NK cell line NK-92MI (#CL-0533; Procell Life Science & Technology Co.) was cultured in the same medium but without IL-2 addition.

Primary NK cells were transfected with siRNA using TransIT-TKO Transfection Reagent (#MIR2152; Mirus Bio; Hargreaves et al., 2020). In brief, ∼1 × 10^6 NK cells were resuspended in 500 µl α-MEM. In a separate microfuge tube, 50 µl α-MEM was combined with 1 µl TKO reagent and 25 nM siRNA and incubated in the dark for 20 min. The α-MEM-TKO-siRNA solution was added dropwise to the cells, and the plate was rocked gently. 18 h later, the cells were collected to assess the knockdown efficiency. All siRNA sequences (Hanbio Biotechnology) used were as follows: mouse-Itga4 sense: 5′-CGGUGAUGCUGUUGUUGUACU-3′; anti-sense: 5′-UACAACAACAGCAUCACCGCU-3′; mouse-VCAM1 sense: 5′-ACUGGGUUGACUUUCAGGUdTSdT-3′; anti-sense: 5′-ACCUGAAAGUCAACCCAGUdTSdT-3′; mouse-Spic sense: 5′-CGCUAGUGUCUGUCAGAAAdTdT-3′; antisense: 5′-UUUCUGACAGACACUAGCGdTdT-3′; and human-Spic sense: 5′-GUGUGUUCAACCUGAUCAAGA-3′; anti-sense: 5′-UUGAUCAGGUUGAACACACUG-3′.

An SE Cell Line 4D-NucleofectorTM X Kit L (#V4XC-1012; Lonza) was used to transfect NK-92MI on an Amaxa Nucleofector II/2b device (Mirusbio). Briefly, ∼1 × 10^6 NK-92MI cells were centrifuged at 1,000 rpm for 5 min, resuspended in 100 µl of the desired electroporation buffer, and mixed with 4 µg of plasmid. The resuspended cells were transferred to cuvettes and immediately electroporated using the program CA-137. After electroporation, the cells were incubated in a cuvette at room temperature for 10 min and then transferred to a 24-well plate containing NK cell culture medium.

Flow cytometry

Mouse NK cells from spleen and liver tissues were analyzed using BD LSRFortessa cell analyzer (BD Biosciences) as previously described (Castro et al., 2018). In brief, single-cell suspensions from the spleen and liver were incubated for ∼30 min on ice with 1% BSA in PBS containing primary antibodies. The primary antibodies were diluted as follows: anti-CD3-allophycocyanin (APC)-cy7 (#100222, 1:200; BioLegend), anti-NK1.1-BV421 (#108732, 1:200; BioLegend), anti-CD11b-FITC (#101206, 1:200; BioLegend), anti-CD27-PE-cy7 (t#124216, 1:200; BioLegend), anti-CD49a-APC (#142606, 1:200; BioLegend), and anti-CD49b-Percp-cy5.5 (#108916, 1:200; BioLegend). The cells were washed twice before analysis. To stain for intracellular antigens, cells were stained for surface antigens, fixed, and permeabilized with Cytofix/Cytoperm (BD Biosciences), washed twice with Cytoperm solution (BD Biosciences), and incubated with anti-IFN-γ-APC (#505809, 1:100; BioLegend). FCS files were exported and analyzed using FlowJo8.3.3 software (TreeStar), and gates were set based on isotype-specific control antibodies. $CD27^+CD11b^+$ (DP) NK cells were obtained from splenic single-cell suspensions by flow cytometry. After the removal of B and T cells with anti-CD19– and anti-CD3–coated beads, respectively, the cells were incubated with diluted primary antibodies as follows: anti-CD3-APC-cy7 (1:200; BioLegend), anti-NK1.1-BV421 (1:200; BioLegend), anti-CD11b-APC (1:200; BioLegend), and anti-CD27-PE-cy7 (1:200; BioLegend). The cells were then washed twice, and sorting was performed using BD FACSAria II flow cytometry system (BD Biosciences).

Histological analysis

After LF induction, the livers were removed and fixed in 10% formaldehyde for 24 h before embedding in paraffin. Sections cut at a thickness of 5 µm were stained with H&E for histological analysis. Sirius red staining was performed according to standard procedures. Quantitative measurement of fibrotic tissue (fibrosis morphometry) was calculated as a percentage of collagen content (Sirius Red–positive area/total area) by digital image analysis using Image-Pro Plus 4.5 software (Media Cybernetics). Six or more fields of each section were measured, and three or more different sections were obtained from each animal (Chen et al., 2017b).

Hydroxyproline assay

To assess collagen synthesis in the fibrotic liver, hepatic hydroxyproline levels were determined using a hydroxyproline assay kit (#A030-2-1; Nanjing Jiancheng Biochemical Institute) according to the manufacturer's instructions. Hydroxyproline content was expressed as µg/mg liver wet weight.

Immunofluorescence

Glass coverslips with cells were fixed in cold acetone and washed with PBS. After permeabilization with PBS containing 0.25% Triton X-100 for 10 min, samples were incubated with 3% BSA in PBS for 30 min to block nonspecific antibody binding and then incubated overnight at 4°C with primary antibodies against NKp46 (#16-3351-81; 1:200; eBioscience) or Spic (#DF3350; 1:200; Affinity), followed by three washes with PBS and incubation with Alexa Fluor 488– or Alexa Fluor 594–conjugated secondary antibodies (Invitrogen) for 2 h at room temperature. As a negative control, species- and isotype-matched IgGs were used instead of primary antibodies. ProLong Gold antifade reagent with DAPI (Invitrogen) was used to mount and counterstain the

specimens, which were subsequently examined using an LSM 800 laser scanning confocal microscope (Carl Zeiss). For F-actin staining, samples were incubated with phalloidin (100 nM) for 20 min at 4°C, rapidly washed three times with buffer, mounted, and viewed.

Cytotoxicity assay

The lactate dehydrogenase release assay was used to determine the cytotoxicity of NK cells against HSCs (Li et al., 2017). Briefly, HSCs were seeded in 96-well plates (~5×10^3 cells per well), and NK cells were subsequently added to HSCs in 96-well plates at an effector:target ratio of 10:1. The plate was incubated for 6 h, and the killing efficiency was measured using the lactate dehydrogenase Cytotoxicity Assay Kit (#C0017; Beyotime) according to the manufacturer's protocol. Cytotoxicity was calculated as follows: cell death ratio (%) = $[(A_{\text{sample}} - A_{control})/(A_{\max} - A_{control})] \times 100$, where A is absorbance value. In some experiments, NK cells and HSCs were incubated for 4 h, and the activated NK cells were labeled with anti-NK 1.1-FITC and anti-IFN-γ-APC and detected by flow cytometry.

Adhesion assay

NK cells adhering to VCAM-1 were cultured as previously described (Kochl et al., 2016). Black 96-well Maxisorp plates (Thermo Fisher Scientific) were coated overnight with 10 µg/ml recombinant VCAM1-Fc (#643-VM) or fibronectin (#4305-FNB; R&D Systems) in PBS at 4°C and blocked with 2% BSA in PBS for 2 h at room temperature. NK cells were labeled with 5 µM CFDA-SE and placed in the wells in PBS and incubated for 4 h at 37°C. The plates were analyzed using a 96-well fluorescence reader (EnSpire 2300 Multilabel Reader; PerkinElmer) to determine the total fluorescence signal per well. After at least three washes with PBS, the fluorescence was measured again, and the percentage of adhesion was calculated by dividing the fluorescence after washing with that before washing.

To evaluate NK/HSC adhesion in vitro (Melhem et al., 2006), early activated HSCs were seeded on round glass coverslips on the bottom of a 24-well plate (~2×10^4 per well), and ~2×10^5 NK cells labeled with CFDA-SE were subsequently added to HSCs per well. After 4 h of incubation, the plates were washed three times to remove nonadherent cells, and the cell slides were observed under a confocal microscope (Carl Zeiss). Adhesion efficiency is expressed as the number of attached NK cells per HSC.

RNA extraction and real-time PCR

Total RNA was isolated from cells using TRIzol reagent (Invitrogen) according to the manufacturer's instructions. RNA concentration and purity were assessed using a NanoDrop 2000 spectrophotometer (Thermo Fisher Scientific). RNA was reverse-transcribed into cDNA using a Reverse Transcription Reagent kit (Takara). The cDNA was amplified for 40 cycles using SYBR Green Universal PCR mix (Takara) on Roche LightCycler 480 Instrument II (Roche). Target gene expression was normalized to the internal control and is presented as the relative expression. The primers used for detection are listed in Table S2.

Western blotting

Proteins from cell and tissue samples were extracted using a lysis buffer containing protease inhibitors. Protein concentration was determined using a bicinchoninic acid Protein Assay Kit (Pierce; Thermo Scientific). Lysates containing equal amounts of protein were separated by 10% SDS-PAGE and transferred to a polyvinylidene difluoride membrane (Millipore). The membrane was incubated with 5% skim milk for 1 h and then incubated with primary antibodies at 4°C overnight. Primary antibodies against the following proteins were used: Spic (#DF3350; 1:1,000; Affinity), α-SMA (#A5228; 1:1,000; Sigma-Aldrich), Desmin (#ab32362; 1:1,000; Abcam), collagen III (#22734-1-AP; 1:1,000; Proteintech), GAPDH (#10494-1-AP; 1:1,000; Proteintech), LaminB (#12987-1-AP; 1:1,000; Proteintech), β-actin (#AC026; 1:100,000; Abclonal), phosphothreonine (#9386S; 1:1,000; Cell Signaling Technology), NKp46 (#A14499; 1:1,000; Abclonal), HA (#51064-2-AP; 1:1,000; Proteintech), and Itga4 (#19676-1-AP; 1:1,000; Proteintech). The membranes were incubated with HRP-labeled secondary antibody (1:2,000; Cell Signaling Technology) in blocking buffer at room temperature for 2 h. Blots were developed using an enhanced chemiluminescence reagent (Thermo Fisher Scientific). The blots were scanned using a Tanon Imaging system (Tanon-5200Multi).

scRNA-seq and analysis

Sorted splenic DP NK cells from two mice (Rivera et al., 2022) from each group ($EP3^{F/F}$ and $NKp46^{Cre}EP3^{F/F}$) were pooled for droplet-based scRNA-seq (10× Genomics platform). Library preparation was performed using the Single Cell 3 v2 kit (10× Genomics) according to the manufacturer's protocol. Sequencing was performed on an Illumina Novaseq 6000 instrument at a depth of 33,185 mean reads per cell. The raw sequencing data of gene expression were aligned with the GRCm39 mouse reference genome using the STAR algorithm in CellRanger software (v3.0.0). Cells with genes having expression values outside the limit of mean value ±2-fold of SD and >10% mitochondrial gene mapped reads were filtered from downstream analyses. Library size normalization was performed in Seurat on the filtered matrix to obtain the normalized count.

The top variable genes across single cells were identified using a previously described method (Macosko et al., 2015). The most variable genes were selected using the FindVariableGenes function in Seurat (Butler et al., 2018). To remove the batch effects in scRNA-seq data (Tran et al., 2020), the mutual nearest neighbors were detected using the R package batchelor (Haghverdi et al., 2018). Graph-based clustering was performed to cluster cells according to their gene expression profiles using the FindClusters function in Seurat. The cells were visualized using a 2D t-SNE algorithm with the RunTSNE function in Seurat. We used the FindAllMarkers function in Seurat to identify the marker genes of each cluster. Then, we used the R package SingleR (Aran et al., 2019), a novel computational method for unbiased cell type recognition of scRNA-seq, with the reference transcriptomic datasets ImmGen (Heng and Painter, 2008) to infer the cell of origin of each single cell independently and identify cell types.

A total of 289 DEGs were identified using the FindMarkers function (test.use = MAST) in Seurat (Butler et al., 2018; Table

S3). A P value <0.05 and $|\log_2$ fold-change$|$ >0.58 were set as the thresholds for significant differential expression. GO enrichment and KEGG pathway enrichment analyses of upregulated genes were performed by Metascape (http://metascape.org/) and DAVID Bioinformatics Resources 6.8 (https://david.ncifcrf.gov/). GSEA was used to complete GO and KEGG term enrichment analysis with the Molecular Signatures Database C5 GO gene sets and C2 KEGG gene sets (v7.2; Subramanian et al., 2005).

SCENIC analysis was run using the motifs database for RcisTarget and GRNboost (SCENIC v1.1.2.2, which corresponds to RcisTarget 1.2.1 and AUCell 1.4.1) with the default parameters (Aibar et al., 2017). In brief, we identified TF binding motifs overrepresented on a gene list using the RcisTarget package. The activity of each group of regulons in each cell was scored using the AUCell package. To evaluate the cell-type specificity of each predicted regulon, we calculated the regulon specificity score, which is based on the Jensen–Shannon divergence, a measure of the similarity between two probability distributions. Specifically, we calculated the Jensen–Shannon divergence between each vector of binary regulon activity overlaps with the assignment of cells to a specific cell type (Suo et al., 2018). The connection specificity index for all regulons was calculated using the scFunctions (https://github.com/FloWuenne/scFunctions/) package. The gene sets used to identify TFs are listed in Table S4. scRNA-seq data have been deposited at the National Center for Biotechnology Information GEO public database under accession no. GSE196864.

Statistical analysis

All data are expressed as the mean ± SEM. Data were analyzed using Prism 5 (GraphPad). The normal distribution of the data was examined using the Shapiro–Wilk normality test. Mann–Whitney *U* tests were used to compare two independent samples. One or two-way ANOVA followed by Tukey test, and Kruskal-Wallis test followed by Dunn's post hoc test, were used for multiple comparisons. Statistical significance was set at $P < 0.05$. Randomization and blinded analyses were performed whenever possible.

Online supplemental material

Fig. S1 shows the effect of EP3 deletion or overexpression on LF in mice with CCL4 treatment. Fig. S2 shows the splenic origin of the hepatic DP NK cells in mice. Fig. S3 shows the accumulation of adoptive transferred DP NK cells in mouse liver tissue. Fig. S4 shows the NK cell markers gene in isolated DP NK cells depicted by t-SNE plot and top 10 genes expressed in each cluster. Fig. S5 shows the effect of overexpression of EP3 on cell adhesion and Spic cytonuclear translocation in DP NK cells. Table S1 shows the clinical characteristics of patients with ALC and healthy controls. Table S2 lists primers for real-time PCR analysis. Table S3 lists the DEGs identified using the FindMarkers function in Seurat. Table S4 lists the gene sets used to identify the TFs in SCENIC analysis.

Acknowledgments

We thank OE Biotech Co., Ltd. (Shanghai, China) for providing scRNA-seq.

This work was supported by the National Key Research and Development Program of China (2018YFA0800601), National Natural Science Foundation of China (81790623, 82030015, 31771269, and 81970540), and Natural Science Foundation of Tianjin (18JCYBJC27300). Y. Yu is a Fellow at the Jiangsu Collaborative Innovation Center for Cardiovascular Disease Translational Medicine.

Author Contributions: Y. Shen and Y. Yu designed the study; X. Tao, R. Zhang, R. Du, H. Yang, J. Li, Y. Wang, Q. Liu, and S. Zuo performed the experiments and provided experimental assistance; X. Tao and T. Yu analyzed the data; Y. Shen wrote the paper. X. Wang, M. Lazarus, L. Zhou, B. Wang, and Y. Yu made critical revision of the manuscript for key intellectual content.

Disclosures: The authors declare no competing financial interests.

Submitted: 2 December 2021
Revised: 7 February 2022
Accepted: 9 March 2022

References

Aibar, S., C.B. Gonzalez-Blas, T. Moerman, V.A. Huynh-Thu, H. Imrichova, G. Hulselmans, F. Rambow, J.C. Marine, P. Geurts, J. Aerts, et al. 2017. SCENIC: Single-cell regulatory network inference and clustering. *Nat. Methods*. 14:1083–1086. https://doi.org/10.1038/nmeth.4463

Allavena, P., G. Bianchi, C. Paganin, G. Giardina, and A. Mantovani. 1996. Regulation of adhesion and transendothelial migration of natural killer cells. *Nat. Immun.* 15:107–116

Aran, D., A.P. Looney, L. Liu, E. Wu, V. Fong, A. Hsu, S. Chak, R.P. Naikawadi, P.J. Wolters, A.R. Abate, et al. 2019. Reference-based analysis of lung single-cell sequencing reveals a transitional profibrotic macrophage. *Nat. Immunol.* 20:163–172. https://doi.org/10.1038/s41590-018-0276-y

Bai, X., J. Wang, Y. Guo, J. Pan, Q. Yang, M. Zhang, H. Li, L. Zhang, J. Ma, F. Shi, et al. 2014. Prostaglandin E2 stimulates β1-integrin expression in hepatocellular carcinoma through the EP1 receptor/PKC/NF-κB pathway. *Sci. Rep.* 4:6538. https://doi.org/10.1038/srep06538

Betz, M., and B.S. Fox. 1991. Prostaglandin E2 inhibits production of Th1 lymphokines but not of Th2 lymphokines. *J. Immunol.* 146:108–113

Biringer, R.G. 2021. A review of prostanoid receptors: Expression, characterization, regulation, and mechanism of action. *J. Cell Commun. Signal.* 15:155–184. https://doi.org/10.1007/s12079-020-00585-0

Bonavita, E., C.P. Bromley, G. Jonsson, V.S. Pelly, S. Sahoo, K. Walwyn-Brown, S. Mensurado, A. Moeini, E. Flanagan, C.R. Bell, et al. 2020. Antagonistic inflammatory phenotypes dictate tumor fate and response to immune checkpoint blockade. *Immunity*. 53:1215–1229.e8.

Bottcher, J.P., E. Bonavita, P. Chakravarty, H. Blees, M. Cabeza-Cabrerizo, S. Sammicheli, N.C. Rogers, E. Sahai, S. Zelenay, and C. Reise Sousa. 2018. NK cells stimulate recruitment of cDC1 into the tumor microenvironment promoting cancer immune control. *Cell*. 172:1022–1037.e14.

Buck, M., G. Garcia-Tsao, R.J. Groszmann, C. Stalling, N.D. Grace, A.K. Burroughs, D. Patch, D.S. Matloff, P. Clopton, and M. Chojkier. 2014. Novel inflammatory biomarkers of portal pressure in compensated cirrhosis patients. *Hepatology*. 59:1052–1059. https://doi.org/10.1002/hep.26755

Butler, A., P. Hoffman, P. Smibert, E. Papalexi, and R. Satija. 2018. Integrating single-cell transcriptomic data across different conditions, technologies, and species. *Nat. Biotechnol.* 36:411–420. https://doi.org/10.1038/nbt.4096

Castro, W., S.T. Chelbi, C. Niogret, C. Ramon-Barros, S.P.M. Welten, K. Osterheld, H. Wang, G. Rota, L. Morgado, E. Vivier, et al. 2018. The transcription factor Rfx7 limits metabolism of NK cells and promotes their maintenance and immunity. *Nat. Immunol.* 19:809–820. https://doi.org/10.1038/s41590-018-0144-9

Chen, D., J. Tang, Q. Wan, J. Zhang, K. Wang, Y. Shen, and Y. Yu. 2017a. E-prostanoid 3 receptor mediates sprouting angiogenesis through suppression of the protein kinase A/β-catenin/notch pathway.

Arterioscler. Thromb. Vasc. Biol. 37:856–866. https://doi.org/10.1161/atvbaha.116.308587

Chen, M., J. Liu, W. Yang, and W. Ling. 2017b. Lipopolysaccharide mediates hepatic stellate cell activation by regulating autophagy and retinoic acid signaling. *Autophagy*. 13:1813–1827. https://doi.org/10.1080/15548627.2017.1356550

Chen, Z., Y. Yang, S.Y. Neo, H. Shi, Y. Chen, A.K. Wagner, K. Larsson, L. Tong, P.J. Jakobsson, E. Alici, et al. 2021. Phosphodiesterase 4A confers resistance to PGE2-mediated suppression in CD25$^+$/CD54$^+$ NK cells. *EMBO Rep.* 22:e51329. https://doi.org/10.15252/embr.202051329

Choi, W.M., T. Ryu, J.H. Lee, Y.R. Shim, M.H. Kim, H.H. Kim, Y.E. Kim, K. Yang, K. Kim, S.E. Choi, et al. 2021. Metabotropic glutamate receptor 5 in natural killer cells attenuates liver fibrosis by exerting cytotoxicity to activated stellate cells. *Hepatology*. 74:2170–2185. https://doi.org/10.1002/hep.31875

Crinier, A., P. Milpied, B. Escaliere, C. Piperoglou, J. Galluso, A. Balsamo, L. Spinelli, I. Cervera-Marzal, M. Ebbo, M. Girard-Madoux, et al. 2018. High-dimensional single-cell analysis identifies organ-specific signatures and conserved NK cell subsets in humans and mice. *Immunity*. 49:971–986.e5. https://doi.org/10.1016/j.immuni.2018.09.009

Dormond, O., M. Bezzi, A. Mariotti, and C. Ruegg. 2002. Prostaglandin E2 promotes integrin alpha Vbeta 3-dependent endothelial cell adhesion, rac-activation, and spreading through cAMP/PKA-dependent signaling. *J. Biol. Chem.* 277:45838–45846. https://doi.org/10.1074/jbc.m209213200

Dormond, O., A. Foletti, C. Paroz, and C. Ruegg. 2001. NSAIDs inhibit alpha V beta 3 integrin-mediated and Cdc42/Rac-dependent endothelial-cell spreading, migration and angiogenesis. *Nat. Med.* 7:1041–1047. https://doi.org/10.1038/nm0901-1041

Ellis, E.L., and D.A. Mann. 2012. Clinical evidence for the regression of liver fibrosis. *J. Hepatol.* 56:1171–1180. https://doi.org/10.1016/j.jhep.2011.09.024

Faggioli, F., E. Palagano, L. Di Tommaso, M. Donadon, V. Marrella, C. Recordati, S. Mantero, A. Villa, P. Vezzoni, and B. Cassani. 2018. B lymphocytes limit senescence-driven fibrosis resolution and favor hepatocarcinogenesis in mouse liver injury. *Hepatology*. 67:1970–1985. https://doi.org/10.1002/hep.29636

Fasbender, F., A. Widera, J.G. Hengstler, and C. Watzl. 2016. Natural killer cells and liver fibrosis. *Front. Immunol.* 7:19. https://doi.org/10.3389/fimmu.2016.00019

Fogler, W.E., K. Volker, K.L. McCormick, M. Watanabe, J.R. Ortaldo, and R.H. Wiltrout. 1996. NK cell infiltration into lung, liver, and subcutaneous B16 melanoma is mediated by VCAM-1/VLA-4 interaction. *J. Immunol.* 156:4707–4714

Fu, B., F. Wang, R. Sun, B. Ling, Z. Tian, and H. Wei. 2011. CD11b and CD27 reflect distinct population and functional specialization in human natural killer cells. *Immunology*. 133:350–359. https://doi.org/10.1111/j.1365-2567.2011.03446.x

Fujita, T., and S. Narumiya. 2016. Roles of hepatic stellate cells in liver inflammation: A new perspective. *Inflamm. Regen.* 36:1. https://doi.org/10.1186/s41232-016-0005-6

Furuta, K., Q. Guo, K.D. Pavelko, J.H. Lee, K.D. Robertson, Y. Nakao, J. Melek, V.H. Shah, P. Hirsova, and S.H. Ibrahim. 2021. Lipid-induced endothelial vascular cell adhesion molecule 1 promotes nonalcoholic steatohepatitis pathogenesis. *J. Clin. Invest.* 131:143690. https://doi.org/10.1172/JCI143690

Galland, S., J. Vuille, P. Martin, I. Letovanec, A. Caignard, G. Fregni, and I. Stamenkovic. 2017. Tumor-derived mesenchymal stem cells use distinct mechanisms to block the activity of natural killer cell subsets. *Cell Rep.* 20:2891–2905. https://doi.org/10.1016/j.celrep.2017.08.089

Glassner, A., M. Eisenhardt, P. Kokordelis, B. Kramer, F. Wolter, H.D. Nischalke, C. Boesecke, T. Sauerbruch, J.K. Rockstroh, U. Spengler, and J. Nattermann. 2013. Impaired CD4$^+$ T cell stimulation of NK cell antifibrotic activity may contribute to accelerated liver fibrosis progression in HIV/HCV patients. *J. Hepatol.* 59:427–433. https://doi.org/10.1016/j.jhep.2013.04.029

Glassner, A., M. Eisenhardt, B. Kramer, C. Korner, M. Coenen, T. Sauerbruch, U. Spengler, and J. Nattermann. 2012. NK cells from HCV-infected patients effectively induce apoptosis of activated primary human hepatic stellate cells in a TRAIL-FasL- and NKG2D-dependent manner. *Lab. Invest.* 92:967–977. https://doi.org/10.1038/labinvest.2012.54

Go, E.M., J.H. Oh, J.H. Park, S.Y. Lee, and N.K. Lee. 2020. Spi-C positively regulates RANKL-mediated osteoclast differentiation and function. *Exp. Mol. Med.* 52:691–701. https://doi.org/10.1038/s12276-020-0427-8

Gomez-Santos, L., Z. Luka, C. Wagner, S. Fernandez-Alvarez, S.C. Lu, J.M. Mato, M.L. Martinez-Chantar, and N. Beraza. 2012. Inhibition of natural killer cells protects the liver against acute injury in the absence of glycine N-methyltransferase. *Hepatology*. 56:747–759. https://doi.org/10.1002/hep.25694

Gur, C., S. Doron, S. Kfir-Erenfeld, E. Horwitz, L. Abu-Tair, R. Safadi, and O. Mandelboim. 2012. NKp46-mediated killing of human and mouse hepatic stellate cells attenuates liver fibrosis. *Gut*. 61:885–893. https://doi.org/10.1136/gutjnl-2011-301400

Haghverdi, L., A.T.L. Lun, M.D. Morgan, and J.C. Marioni. 2018. Batch effects in single-cell RNA-sequencing data are corrected by matching mutual nearest neighbors. *Nat. Biotechnol.* 36:421–427. https://doi.org/10.1038/nbt.4091

Haldar, M., M. Kohyama, A.L. So, A.Y. So, W. Kc, X. Wu, C. Briseño, C.G. Briseno, A. Satpathy, A.T. Satpathy, et al. 2014. Heme-mediated SPI-C induction promotes monocyte differentiation into iron-recycling macrophages. *Cell*. 156:1223–1234. https://doi.org/10.1016/j.cell.2014.01.069

Hargreaves, B.K.V., S.E. Roberts, B. Derfalvi, and J.E. Boudreau. 2020. Highly efficient serum-free manipulation of miRNA in human NK cells without loss of viability or phenotypic alterations is accomplished with TransIT-TKO. *PLoS One*. 15:e0231664. https://doi.org/10.1371/journal.pone.0231664

Harizi, H., J.B. Corcuff, and N. Gualde. 2008. Arachidonic-acid-derived eicosanoids: Roles in biology and immunopathology. *Trends Mol. Med.* 14:461–469. https://doi.org/10.1016/j.molmed.2008.08.005

Hayashi, K., F. Nikolos, Y.C. Lee, A. Jain, E. Tsouko, H. Gao, A. Kasabyan, H.E. Leung, A. Osipov, S.Y. Jung, et al. 2020. Tipping the immunostimulatory and inhibitory DAMP balance to harness immunogenic cell death. *Nat. Commun.* 11:6299. https://doi.org/10.1038/s41467-020-19970-9

Helander, T.S., and T. Timonen. 1998. Adhesion in NK cell function. *Curr. Top. Microbiol. Immunol.* 230:89–99. https://doi.org/10.1007/978-3-642-46859-9_7

Heng, T.S., and M.W. Painter. 2008. The immunological genome project: Networks of gene expression in immune cells. *Nat. Immunol.* 9:1091–1094. https://doi.org/10.1038/ni1008-1091

Henkel, J., C.D. Coleman, A. Schraplau, K. Johrens, T.S. Weiss, W. Jonas, A. Schurmann, and G.P. Puschel. 2018. Augmented liver inflammation in a microsomal prostaglandin E synthase 1 (mPGES-1)-deficient diet-induced mouse NASH model. *Sci. Rep.* 8:16127. https://doi.org/10.1038/s41598-018-34633-y

Higashi, T., S.L. Friedman, and Y. Hoshida. 2017. Hepatic stellate cells as key target in liver fibrosis. *Adv. Drug Deliv. Rev.* 121:27–42. https://doi.org/10.1016/j.addr.2017.05.007

Hoggatt, J., P. Singh, J. Sampath, and L.M. Pelus. 2009. Prostaglandin E2 enhances hematopoietic stem cell homing, survival, and proliferation. *Blood*. 113:5444–5455. https://doi.org/10.1182/blood-2009-01-201335

Holt, D., X. Ma, N. Kundu, and A. Fulton. 2011. Prostaglandin E(2) (PGE (2)) suppresses natural killer cell function primarily through the PGE(2) receptor EP4. *Cancer Immunol. Immunother.* 60:1577–1586. https://doi.org/10.1007/s00262-011-1064-9

Holt, D.M., X. Ma, N. Kundu, P.D. Collin, and A.M. Fulton. 2012. Modulation of host natural killer cell functions in breast cancer via prostaglandin E2 receptors EP2 and EP4. *J. Immunother.* 35:179–188. https://doi.org/10.1097/CJI.0b013e318247a5e9

Huang, D.W., B.T. Sherman, and R.A. Lempicki. 2009. Systematic and integrative analysis of large gene lists using DAVID bioinformatics resources. *Nat. Protoc.* 4:44–57. https://doi.org/10.1038/nprot.2008.211

Hui, A.Y., A.J. Dannenberg, J.J. Sung, K. Subbaramaiah, B. Du, P. Olinga, and S.L. Friedman. 2004. Prostaglandin E2 inhibits transforming growth factor beta 1-mediated induction of collagen alpha 1(I) in hepatic stellate cells. *J. Hepatol.* 41:251–258. https://doi.org/10.1016/j.jhep.2004.04.033

Kahraman, A., F.J. Barreyro, S.F. Bronk, N.W. Werneburg, J.L. Mott, Y. Akazawa, H.C. Masuoka, C.L. Howe, and G.J. Gores. 2008. TRAIL mediates liver injury by the innate immune system in the bile duct-ligated mouse. *Hepatology*. 47:1317–1330. https://doi.org/10.1002/hep.22136

Kisseleva, T., and D. Brenner. 2021. Molecular and cellular mechanisms of liver fibrosis and its regression. *Nat. Rev. Gastroenterol. Hepatol.* 18:151–166. https://doi.org/10.1038/s41575-020-00372-7

Kochl, R., F. Thelen, L. Vanes, T.F. Brazao, K. Fountain, J. Xie, C.L. Huang, R. Lyck, J.V. Stein, and V.L. Tybulewicz. 2016. WNK1 kinase balances T cell adhesion versus migration in vivo. *Nat. Immunol.* 17:1075–1083. https://doi.org/10.1038/ni.3495

Kohyama, M., W. Ise, B.T. Edelson, P.R. Wilker, K. Hildner, C. Mejia, W.A. Frazier, T.L. Murphy, and K.M. Murphy. 2009. Role for Spi-C in the development of red pulp macrophages and splenic iron homeostasis. *Nature*. 457:318–321. https://doi.org/10.1038/nature07472

Krause, P., M. Bruckner, C. Uermosi, E. Singer, M. Groettrup, and D.F. Legler. 2009. Prostaglandin E(2) enhances T-cell proliferation by inducing the costimulatory molecules OX40L, CD70, and 4-1BBL on dendritic cells. *Blood*. 113:2451–2460. https://doi.org/10.1182/blood-2008-05-157123

Krizhanovsky, V., M. Yon, R.A. Dickins, S. Hearn, J. Simon, C. Miething, H. Yee, L. Zender, and S.W. Lowe. 2008. Senescence of activated stellate cells limits liver fibrosis. *Cell*. 134:657–667. https://doi.org/10.1016/j.cell.2008.06.049

Laramee, A.S., H. Raczkowski, P. Shao, C. Batista, D. Shukla, L. Xu, S.M.M. Haeryfar, Y. Tesfagiorgis, S. Kerfoot, and R. DeKoter. 2020. Opposing roles for the related ETS-family transcription factors Spi-B and Spi-C in regulating B cell differentiation and function. *Front. Immunol.* 11:841. https://doi.org/10.3389/fimmu.2020.00841

Lazarus, M., K. Yoshida, R. Coppari, C.E. Bass, T. Mochizuki, B.B. Lowell, and C.B. Saper. 2007. EP3 prostaglandin receptors in the median preoptic nucleus are critical for fever responses. *Nat. Neurosci.* 10:1131–1133. https://doi.org/10.1038/nn1949

Li, Y., M. Liu, Z. Zuo, J. Liu, X. Yu, Y. Guan, R. Zhan, Q. Han, J. Zhang, R. Zhou, et al. 2017. TLR9 regulates the NF-κB-NLRP3-IL-1β pathway negatively in salmonella-induced NKG2D-mediated intestinal inflammation. *J. Immunol.* 199:761–773. https://doi.org/10.4049/jimmunol.1601416

Li, Y.M., and J.G. Fan. 2019. Guidelines of prevention and treatment for alcoholic liver disease (2018, China). *J. Dig. Dis.* 20:174–180. https://doi.org/10.1111/1751-2980.12687

Liu, J.F., Y.C. Fong, C.S. Chang, C.Y. Huang, H.T. Chen, W.H. Yang, C.J. Hsu, L.B. Jeng, C.Y. Chen, and C.H. Tang. 2010. Cyclooxygenase-2 enhances alpha2beta1 integrin expression and cell migration via EP1 dependent signaling pathway in human chondrosarcoma cells. *Mol. Cancer*. 9:43. https://doi.org/10.1186/1476-4598-9-43

Liu, Q., H. Zhang, X. Tian, L. He, X. Huang, Z. Tan, Y. Yan, S.M. Evans, J.D. Wythe, and B. Zhou. 2016. Smooth muscle origin of postnatal 2nd CVP is pre-determined in early embryo. *Biochem. Biophys. Res. Commun.* 471:430–436. https://doi.org/10.1016/j.bbrc.2016.02.062

Lukacs-Kornek, V., and D. Schuppan. 2013. Dendritic cells in liver injury and fibrosis: Shortcomings and promises. *J. Hepatol.* 59:1124–1126. https://doi.org/10.1016/j.jhep.2013.05.033

Ma, M., S. Badeti, K. Geng, and D. Liu. 2020. Efficacy of targeting SARS-CoV-2 by CAR-NK cells. *bioRxiv*. https://doi.org/10.1101/2020.08.11.247320

Mace, E.M., P. Dongre, H.T. Hsu, P. Sinha, A.M. James, S.S. Mann, L.R. Forbes, L.B. Watkin, and J.S. Orange. 2014. Cell biological steps and checkpoints in accessing NK cell cytotoxicity. *Immunol. Cell Biol.* 92:245–255. https://doi.org/10.1038/icb.2013.96

Macosko, E.Z., A. Basu, R. Satija, J. Nemesh, K. Shekhar, M. Goldman, I. Tirosh, A.R. Bialas, N. Kamitaki, E.M. Martersteck, et al. 2015. Highly parallel genome-wide expression profiling of individual cells using nanoliter droplets. *Cell*. 161:1202–1214. https://doi.org/10.1016/j.cell.2015.05.002

Marcellin, P., E. Gane, M. Buti, N. Afdhal, W. Sievert, I.M. Jacobson, M.K. Washington, G. Germanidis, J.F. Flaherty, R. Aguilar Schall, et al. 2013. Regression of cirrhosis during treatment with tenofovir disoproxil fumarate for chronic hepatitis B: A 5-year open-label follow-up study. *Lancet*. 381:468–475. https://doi.org/10.1016/S0140-6736(12)61425-1

Martinet, L., C. Jean, G. Dietrich, J.J. Fournie, and R. Poupot. 2010. PGE2 inhibits natural killer and gamma delta T cell cytotoxicity triggered by NKR and TCR through a cAMP-mediated PKA type I-dependent signaling. *Biochem. Pharmacol.* 80:838–845. https://doi.org/10.1016/j.bcp.2010.05.002

Massoumi, R., C.K. Nielsen, D. Azemovic, and A. Sjolander. 2003. Leukotriene D4-induced adhesion of Caco-2 cells is mediated by prostaglandin E2 and upregulation of alpha2beta1-integrin. *Exp. Cell Res.* 289:342–351. https://doi.org/10.1016/s0014-4827(03)00285-4

Mayoral, R., A. Fernandez-Martinez, L. Bosca, and P. Martin-Sanz. 2005. Prostaglandin E2 promotes migration and adhesion in hepatocellular carcinoma cells. *Carcinogenesis*. 26:753–761. https://doi.org/10.1093/carcin/bgi022

Mederacke, I., D.H. Dapito, S. Affo, H. Uchinami, and R.F. Schwabe. 2015. High-yield and high-purity isolation of hepatic stellate cells from normal and fibrotic mouse livers. *Nat. Protoc.* 10:305–315. https://doi.org/10.1038/nprot.2015.017

Melder, R.J., G.C. Koenig, B.P. Witwer, N. Safabakhsh, L.L. Munn, and R.K. Jain. 1996. During angiogenesis, vascular endothelial growth factor and basic fibroblast growth factor regulate natural killer cell adhesion to tumor endothelium. *Nat. Med.* 2:992–997. https://doi.org/10.1038/nm0996-992

Mele, D., B. Oliviero, S. Mantovani, S. Ludovisi, A. Lombardi, F. Genco, R. Gulminetti, S. Novati, M.U. Mondelli, and S. Varchetta. 2021. Adaptive natural killer cell functional recovery in hepatitis C virus cured patients. *Hepatology*. 73:79–90. https://doi.org/10.1002/hep.31273

Melhem, A., N. Muhanna, A. Bishara, C.E. Alvarez, Y. Ilan, T. Bishara, A. Horani, M. Nassar, S.L. Friedman, and R. Safadi. 2006. Anti-fibrotic activity of NK cells in experimental liver injury through killing of activated HSC. *J. Hepatol.* 45:60–71. https://doi.org/10.1016/j.jhep.2005.12.025

Mitra, A., A. Satelli, J. Yan, X. Xueqing, M. Gagea, C.A. Hunter, L. Mishra, and S. Li. 2014. IL-30 (IL27p28) attenuates liver fibrosis through inducing NKG2D-rae1 interaction between NKT and activated hepatic stellate cells in mice. *Hepatology*. 60:2027–2039. https://doi.org/10.1002/hep.27392

Moreno-Layseca, P., J. Icha, H. Hamidi, and J. Ivaska. 2019. Integrin trafficking in cells and tissues. *Nat. Cell Biol.* 21:122–132. https://doi.org/10.1038/s41556-018-0223-z

Muhanna, N., S. Doron, O. Wald, A. Horani, A. Eid, O. Pappo, S.L. Friedman, and R. Safadi. 2008. Activation of hepatic stellate cells after phagocytosis of lymphocytes: A novel pathway of fibrogenesis. *Hepatology*. 48:963–977. https://doi.org/10.1002/hep.22413

Nakamoto, S., Y. Ito, N. Nishizawa, T. Goto, K. Kojo, Y. Kumamoto, M. Watanabe, S. Narumiya, and M. Majima. 2020. EP3 signaling in dendritic cells promotes liver repair by inducing IL-13-mediated macrophage differentiation in mice. *FASEB J.* 34:5610–5627. https://doi.org/10.1096/fj.201901955R

Novobrantseva, T.I., G.R. Majeau, A. Amatucci, S. Kogan, I. Brenner, S. Casola, M.J. Shlomchik, V. Koteliansky, P.S. Hochman, and A. Ibraghimov. 2005. Attenuated liver fibrosis in the absence of B cells. *J. Clin. Invest.* 115:3072–3082. https://doi.org/10.1172/jci24798

Okreglicka, K., I. Iten, L. Pohlmeier, L. Onder, Q. Feng, M. Kurrer, B. Ludewig, P. Nielsen, C. Schneider, and M. Kopf. 2021. PPARγ is essential for the development of bone marrow erythroblastic island macrophages and splenic red pulp macrophages. *J. Exp. Med.* 218:e20191314

Osborn, L., C. Vassallo, and C.D. Benjamin. 1992. Activated endothelium binds lymphocytes through a novel binding site in the alternately spliced domain of vascular cell adhesion molecule-1. *J. Exp. Med.* 176:99–107. https://doi.org/10.1084/jem.176.1.99

Pan, J., Q. Yang, J. Shao, L. Zhang, J. Ma, Y. Wang, B.H. Jiang, J. Leng, and X. Bai. 2016. Cyclooxygenase-2 induced β1-integrin expression in NSCLC and promoted cell invasion via the EP1/MAPK/E2F-1/FoxC2 signal pathway. *Sci. Rep.* 6:33823. https://doi.org/10.1038/srep33823

Park, O., W.I. Jeong, L. Wang, H. Wang, Z.X. Lian, M.E. Gershwin, and B. Gao. 2009. Diverse roles of invariant natural killer T cells in liver injury and fibrosis induced by carbon tetrachloride. *Hepatology*. 49:1683–1694. https://doi.org/10.1002/hep.22813

Pellicoro, A., P. Ramachandran, J.P. Iredale, and J.A. Fallowfield. 2014. Liver fibrosis and repair: Immune regulation of wound healing in a solid organ. *Nat. Rev. Immunol.* 14:181–194. https://doi.org/10.1038/nri3623

Radaeva, S., R. Sun, B. Jaruga, V.T. Nguyen, Z. Tian, and B. Gao. 2006. Natural killer cells ameliorate liver fibrosis by killing activated stellate cells in NKG2D-dependent and tumor necrosis factor-related apoptosis-inducing ligand-dependent manners. *Gastroenterology*. 130:435–452. https://doi.org/10.1053/j.gastro.2005.10.055

Radaeva, S., L. Wang, S. Radaev, W.I. Jeong, O. Park, and B. Gao. 2007. Retinoic acid signaling sensitizes hepatic stellate cells to NK cell killing via upregulation of NK cell activating ligand RAE1. *Am. J. Physiol. Gastrointest. Liver Physiol.* 293:G809–G816. https://doi.org/10.1152/ajpgi.00212.2007

Ramirez, P., M.P. Rettig, G.L. Uy, E. Deych, M.S. Holt, J.K. Ritchey, and J.F. DiPersio. 2009. BIO5192, a small molecule inhibitor of VLA-4, mobilizes hematopoietic stem and progenitor cells. *Blood*. 114:1340–1343. https://doi.org/10.1182/blood-2008-10-184721

Rivera, C.A., V. Randrian, W. Richer, Y. Gerber-Ferder, M.G. Delgado, A.S. Chikina, A. Frede, C. Sorini, M. Maurin, H. Kammoun-Chaari, et al. 2022. Epithelial colonization by gut dendritic cells promotes their functional diversification. *Immunity*. 55:129–144.e8. https://doi.org/10.1016/j.immuni.2021.11.008

Rurik, J.G., I. Tombacz, A. Yadegari, P.O. Mendez Fernandez, S.V. Shewale, L. Li, T. Kimura, O.Y. Soliman, T.E. Papp, Y.K. Tam, et al. 2022. CAR T cells produced in vivo to treat cardiac injury. *Science*. 375:91–96. https://doi.org/10.1126/science.abm0594

Sakanaka, M., S. Tanaka, Y. Sugimoto, and A. Ichikawa. 2008. Essential role of EP3 subtype in prostaglandin E2-induced adhesion of mouse cultured and peritoneal mast cells to the Arg-Gly-Asp-enriched matrix. *Am. J. Physiol. Cell Physiol.* 295:C1427–C1433. https://doi.org/10.1152/ajpcell.00218.2008

Schippers, M., L. Beljaars, E. Post, S. Lotersztajn, C. Reker-Smit, B. Han, P. Munoz-Llancao, M. Schmidt, and K. Poelstra. 2017. Upregulation of Epac-1 in hepatic stellate cells by prostaglandin E2 in liver fibrosis is associated with reduced fibrogenesis. *J. Pharmacol. Exp. Ther.* 363: 126–135. https://doi.org/10.1124/jpet.117.241646

Shannon, M.J., and E.M. Mace. 2021. Natural killer cell integrins and their functions in tissue residency. *Front. Immunol.* 12:647358. https://doi.org/10.3389/fimmu.2021.647358

Shen, H., L. Sheng, Y. Xiong, Y.H. Kim, L. Jiang, Z. Chen, Y. Liu, K. Pyaram, C.H. Chang, and L. Rui. 2017. Thymic NF-kappaB-inducing kinase regulates $CD4^+$ T cell-elicited liver injury and fibrosis in mice. *J. Hepatol.* 67:100–109. https://doi.org/10.1016/j.jhep.2017.02.025

Sojka, D.K., B. Plougastel-Douglas, L. Yang, M.A. Pak-Wittel, M.N. Artyomov, Y. Ivanova, C. Zhong, J.M. Chase, P.B. Rothman, J. Yu, et al. 2014. Tissue-resident natural killer (NK) cells are cell lineages distinct from thymic and conventional splenic NK cells. *Elife.* 3:e01659. https://doi.org/10.7554/eLife.01659

Solé, C., E. Sola, M. Morales-Ruiz, G. Fernandez, P. Huelin, I. Graupera, R. Moreira, G. de Prada, X. Ariza, E. Pose, et al. 2016. Characterization of inflammatory response in acute-on-chronic liver failure and relationship with prognosis. *Sci. Rep.* 6:32341. https://doi.org/10.1038/srep32341

Subramanian, A., P. Tamayo, V.K. Mootha, S. Mukherjee, B.L. Ebert, M.A. Gillette, A. Paulovich, S.L. Pomeroy, T.R. Golub, E.S. Lander, and J.P. Mesirov. 2005. Gene set enrichment analysis: A knowledge-based approach for interpreting genome-wide expression profiles. *Proc. Natl. Acad. Sci. USA.* 102:15545–15550. https://doi.org/10.1073/pnas.0506580102

Suh, Y.G., J.K. Kim, J.S. Byun, H.S. Yi, Y.S. Lee, H.S. Eun, S.Y. Kim, K.H. Han, K.S. Lee, G. Duester, et al. 2012. $CD11b^+$ $Gr1^+$ bone marrow cells ameliorate liver fibrosis by producing interleukin-10 in mice. *Hepatology.* 56:1902–1912. https://doi.org/10.1002/hep.25817

Suo, S., Q. Zhu, A. Saadatpour, L. Fei, G. Guo, and G.C. Yuan. 2018. Revealing the critical regulators of cell identity in the mouse cell atlas. *Cell Rep.* 25: 1436–1445.e3. https://doi.org/10.1016/j.celrep.2018.10.045

Tacke, F., and H.W. Zimmermann. 2014. Macrophage heterogeneity in liver injury and fibrosis. *J. Hepatol.* 60:1090–1096. https://doi.org/10.1016/j.jhep.2013.12.025

Tang, J., Y. Shen, G. Chen, Q. Wan, K. Wang, J. Zhang, J. Qin, G. Liu, S. Zuo, B. Tao, et al. 2017. Activation of E-prostanoid 3 receptor in macrophages facilitates cardiac healing after myocardial infarction. *Nat. Commun.* 8: 14656. https://doi.org/10.1038/ncomms14656

Taylor, A.E., A.N. Carey, R. Kudira, C.S. Lages, T. Shi, S. Lam, R. Karns, J. Simmons, K. Shanmukhappa, M. Almanan, et al. 2018. Interleukin 2 promotes hepatic regulatory T cell responses and protects from biliary fibrosis in murine sclerosing cholangitis. *Hepatology.* 68:1905–1921. https://doi.org/10.1002/hep.30061

Tran, H.T.N., K.S. Ang, M. Chevrier, X. Zhang, N.Y.S. Lee, M. Goh, and J. Chen. 2020. A benchmark of batch-effect correction methods for single-cell RNA sequencing data. *Genome Biol.* 21:12. https://doi.org/10.1186/s13059-019-1850-9

Wehr, A., C. Baeck, F. Heymann, P.M. Niemietz, L. Hammerich, C. Martin, H.W. Zimmermann, O. Pack, N. Gassler, K. Hittatiya, et al. 2013. Chemokine receptor CXCR6-dependent hepatic NK T Cell accumulation promotes inflammation and liver fibrosis. *J. Immunol.* 190:5226–5236. https://doi.org/10.4049/jimmunol.1202909

Yao, C., D. Sakata, Y. Esaki, Y. Li, T. Matsuoka, K. Kuroiwa, Y. Sugimoto, and S. Narumiya. 2009. Prostaglandin E2-EP4 signaling promotes immune inflammation through Th1 cell differentiation and Th17 cell expansion. *Nat. Med.* 15:633–640. https://doi.org/10.1038/nm.1968

Yu, M., Z. Su, X. Huang, Y. Zhou, X. Zhang, B. Wang, Z. Wang, Y. Liu, N. Xing, M. Xia, and X. Wang. 2021. Histone methyltransferase Ezh2 negatively regulates NK cell terminal maturation and function. *J. Leukoc. Biol.* 110: 1033–1045. https://doi.org/10.1002/JLB.1MA0321-155RR

Zaslona, Z., C.H. Serezani, K. Okunishi, D.M. Aronoff, and M. Peters-Golden. 2012. Prostaglandin E2 restrains macrophage maturation via E prostanoid receptor 2/protein kinase A signaling. *Blood.* 119:2358–2367. https://doi.org/10.1182/blood-2011-08-374207

Zhang, Q.F., W.W. Yin, Y. Xia, Y.Y. Yi, Q.F. He, X. Wang, H. Ren, and D.Z. Zhang. 2017. Liver-infiltrating $CD11b^-CD27^-$ NK subsets account for NK-cell dysfunction in patients with hepatocellular carcinoma and are associated with tumor progression. *Cell Mol Immunol.* 14:819–829. https://doi.org/10.1038/cmi.2016.28

JEM

Supplemental material

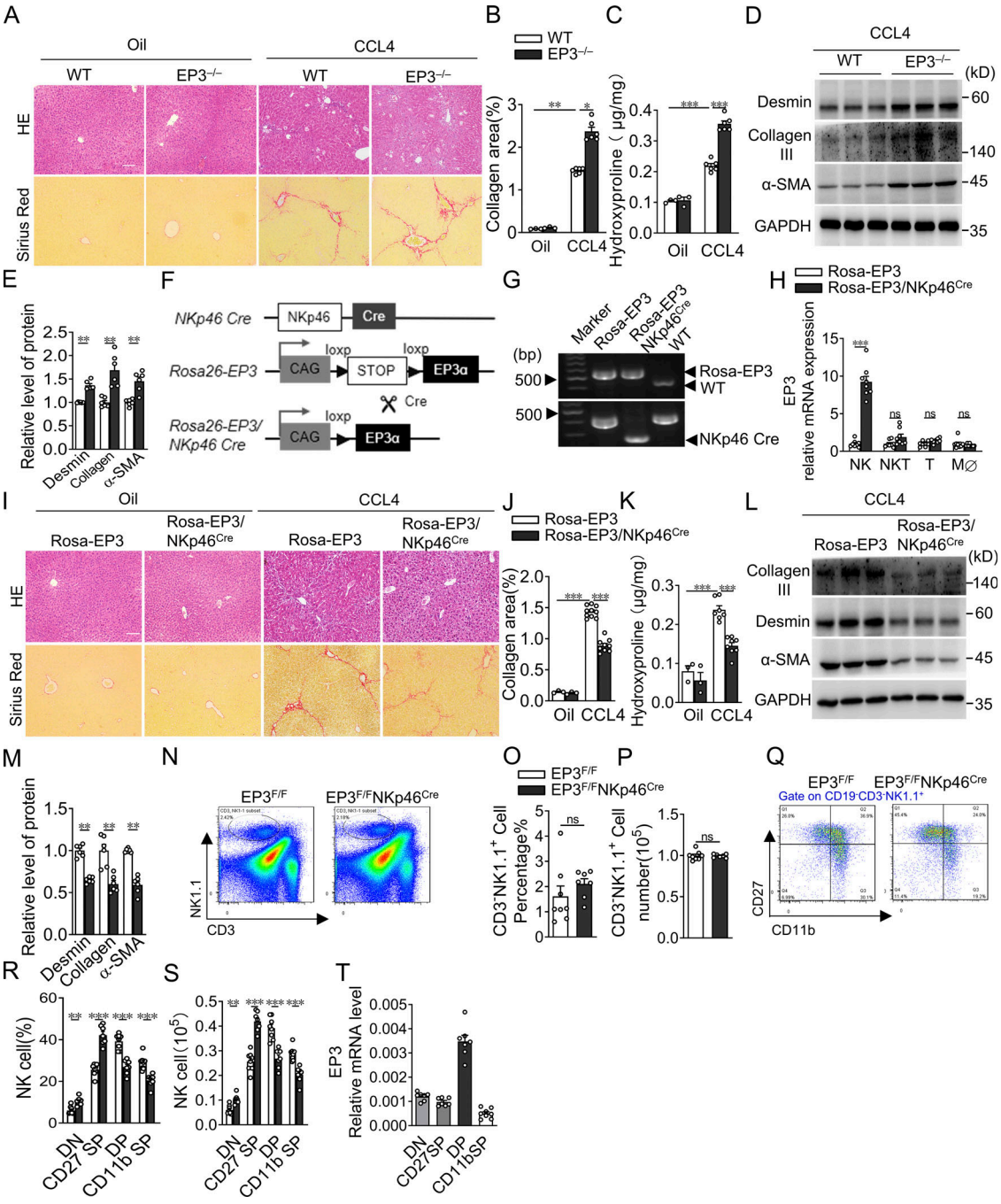

Figure S1. **EP3 is required for NK cell–mediated protection against LF in mice. (A)** H&E and Sirius red staining of CCL4-treated livers from WT and EP3$^{-/-}$ mice. Scale bars, 100 µm. **(B)** Quantification of Sirius red–stained collagen in A (oil, *n* = 3 per group; CCL4, *n* = 6 per group). **(C)** Quantification of hepatic hydroxyproline in CCL4-treated liver from WT and EP3$^{-/-}$ mice (oil, *n* = 3 per group; CCL4, *n* = 6 per group). **(D)** Western blot analysis of protein levels of α-SMA, collagen III, and desmin in CCL4-treated livers from WT and EP3$^{-/-}$ mice. **(E)** Quantification of protein levels in D (*n* = 6 per group). **(F)** Schematic diagram for the generation of Rosa-EP3/NKp46^{Cre} mice. **(G)** Genotyping of NK cell–specific EP3 overexpressed mice by PCR of genomic DNA extracted from the tail biopsies. **(H)** Quantification of EP3 expression in NK cells, NKT cells, T cells, and macrophages from Rosa-EP3 and Rosa-EP3/NKp46^{Cre} mice (*n* = 8 per group). **(I)** H&E and Sirius red staining of CCL4-treated liver from Rosa-EP3 and Rosa-EP3/NKp46^{Cre} mice. Scale bars, 100 µm. **(J)** Quantification of Sirius red–stained collagen in I (oil, *n* = 3 per group; CCL4, *n* = 9–10 per group). **(K)** Quantification of hepatic hydroxyproline in CCL4-treated liver from Rosa-EP3 and Rosa-EP3/NKp46^{Cre} mice (oil, *n* = 3 per group; CCL4, *n* = 7–8 per group). **(L)** Western blot analysis of protein levels of α-SMA, collagen III, and desmin in CCL4-treated liver from Rosa-EP3 and Rosa-EP3/NKp46^{Cre} mice. **(M)** Quantification of protein levels in L (*n* = 6 per group). **(N–P)** Representative flow cytometric image (N), percentages (O), and numbers (P) of NK1.1^{+} hepatic NK cells, depicted for EP3$^{F/F}$ and EP3$^{F/F}$NKp46^{Cre} mice with CCL4 treatment for 10 d (*n* = 7–8 per group). **(Q–S)** Representative flow cytometric image (Q), percentages (R), and numbers (S) of four-stage development of hepatic NK cells, depicted for EP3$^{F/F}$ and EP3$^{F/F}$NKp46^{Cre} mice challenged with CCL4 (*n* = 7–8 per group). **(T)** Relative expression of EP3 in NK subsets (*n* = 7–8 per group). Data are representative of two independent experiments (A–E and G–T). Data represent mean ± SEM. Statistical significance was evaluated by two-way ANOVA followed by Tukey's test for multiple comparisons (B, C, J, and K) and Mann–Whitney *U* test (E, H, M, R, and S). *, P < 0.05; **, P < 0.01; ***, P < 0.001. Source data are available for this figure: SourceData FS1.

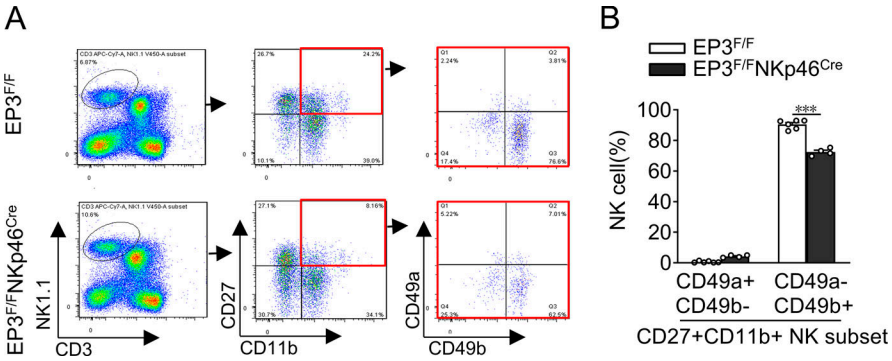

Figure S2. **Hepatic DP NK cells are largely CD49a⁻CD49b⁺ splenic NK cells. (A and B)** Representative flow cytometric profiles (A) and percentages (B) of CD49a⁻CD49b⁺ population in hepatic DP NK cells (gated as NK1.1⁺CD3⁻CD19⁻) from EP3$^{F/F}$ and EP3$^{F/F}$NKp46^{Cre} mice (n = 4–6 per group). Data are representative of two independent experiments. Data represent mean ± SEM. Statistical significance was evaluated by two-way ANOVA followed by Tukey's test for multiple comparisons (B). ***, P < 0.001.

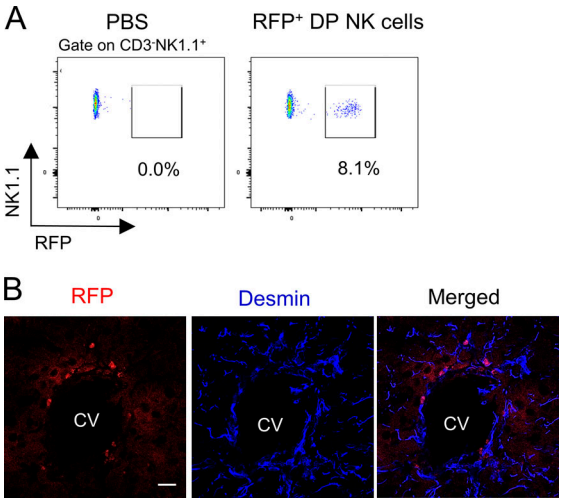

Figure S3. **Adoptive transfer of DP NK cells. (A)** Flow cytometry analysis of transferred NK cells in CCL4-treated mouse liver on day 5 after cell injection. **(B)** Representative immunofluorescence image of adoptive transferred DP NK cells in liver tissue. Scale bars, 20 µm. Data are representative of two independent experiments.

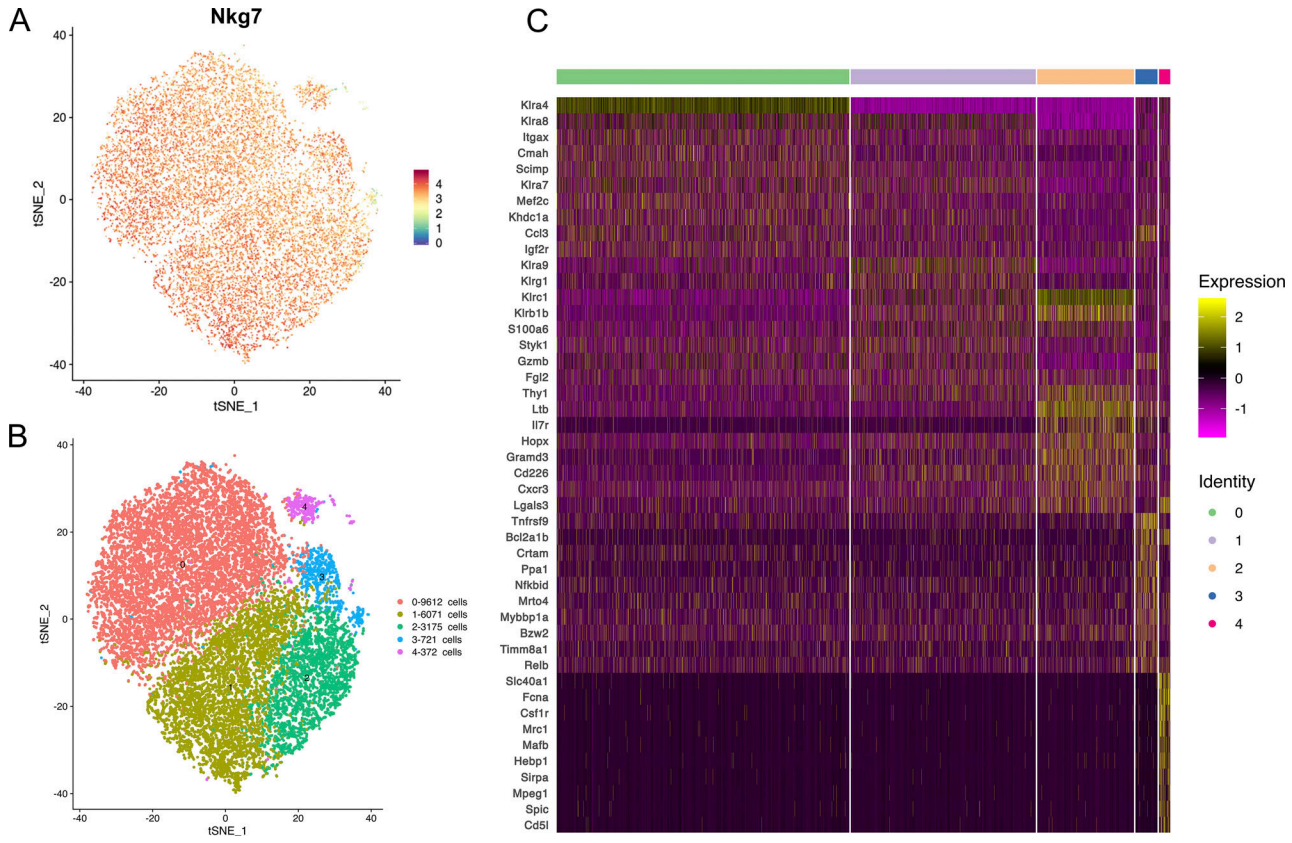

Figure S4. **Cell type identification of isolated DP NK cells. (A)** t-SNE plots depicting NK cell marker gene Nkg7 in isolated DP NK cells. **(B)** t-SNE plots of isolated DP NK cells determined by Seurat. A total of five clusters (clusters 0–4) were identified and color-coded. **(C)** Heatmap of the top 10 genes expressed in each cluster. Cells are grouped by clusters.

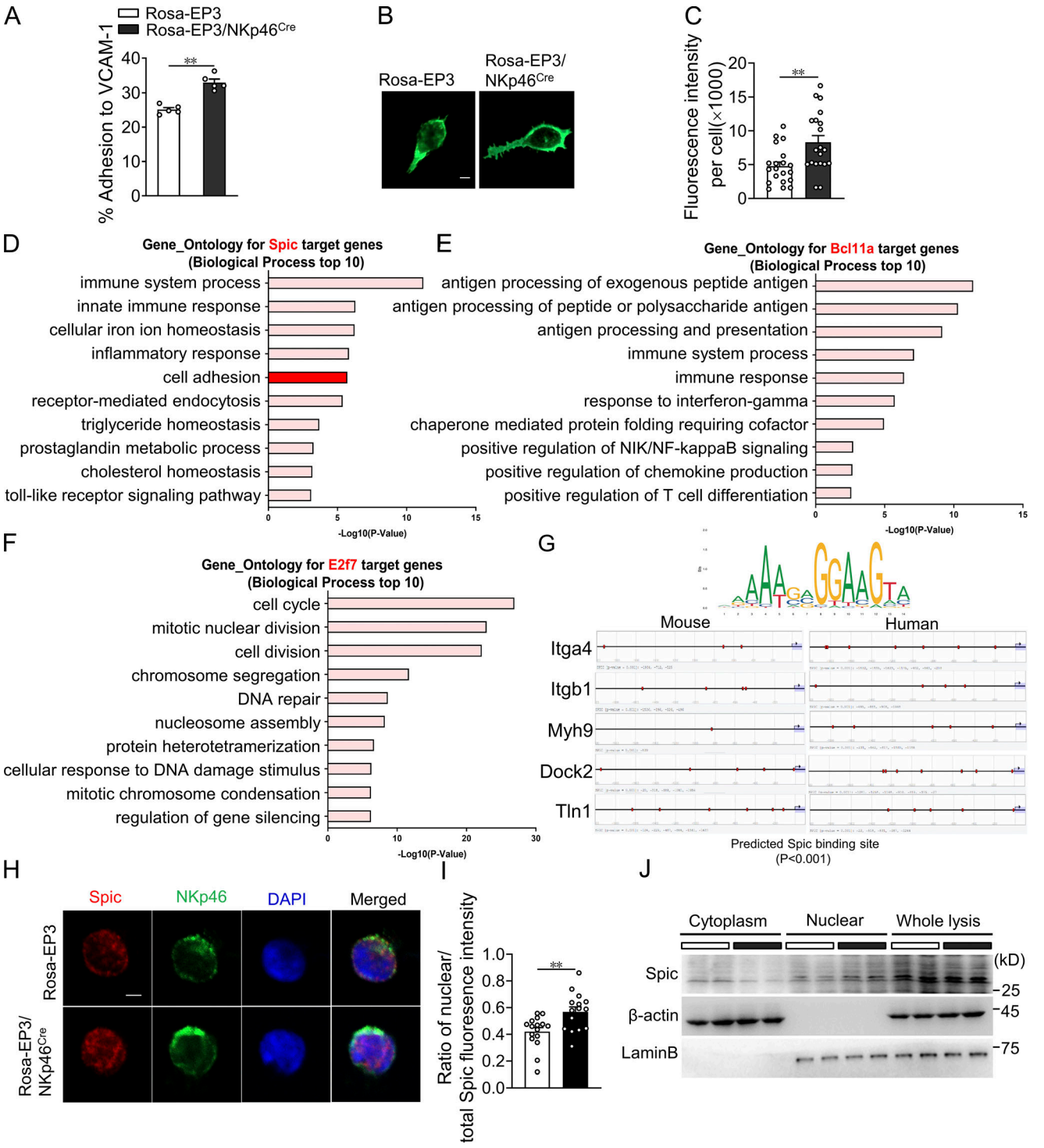

Figure S5. **EP3 enhances the adhesion of DP NK cells via Spic. (A)** Ratio of cell adhesion to plate-bound VCAM-1 in control and EP3-overexpressed DP NK cells (n = 5 per group). **(B)** Immunofluorescence images of F-actin stained with phalloidin in control and EP3-overexpressed DP NK cells. Scale bars, 2 µm. **(C)** Quantification of the density of F-actin filaments in B (n = 20 per group). **(D–F)** Top 10 enriched GO terms (BP) in target genes of Spic (D), Bcl11a (E), and E2F7 (F). **(G)** Predicted binding site of Spic on mouse *Itga4*, *Tln1*, *Dock2*, *Itgb1*, and *Mhy9* promoters by JASPAR. **(H and I)** Representative immunofluorescence images (H) and ratio (I) of nuclear distribution of Spic in control and EP3 overexpressed DP NK cells (n = 15–16 per group). Scale bars, 2 µm. **(J)** Western blot assay of cytosol-nuclear distribution of Spic in DP NK cells. Data are representative of two independent experiments (A–C and H–J). Data represent mean ± SEM. Statistical significance was evaluated by Mann–Whitney U test (A, C, and I). **, P < 0.01.Source data are available for this figure: SourceData FS5.

Provided online are four tables. Table S1 shows the clinical characteristics of patients with ALC and healthy controls. Table S2 lists primers for real-time PCR analysis. Table S3 lists the DEGs identified using the FindMarkers function in Seurat. Table S4 lists the gene sets used to identify the TFs in SCENIC analysis.